

# Dynamics of rotation in M dwarfs: Indications for a change in the dynamo regime in stars at the onset of complete convection<sup>1</sup>

E.R. Houdebine<sup>1</sup>

*Armagh Observatory, College Hill, BT61 9DG Armagh, Northern Ireland*  
and

D.J. Mullan<sup>2</sup>

*Department of Physics and Astronomy, University of Delaware, Newark, DE 19716, USA*

## ABSTRACT

We have measured  $v \sin i$  with high precision for a sample of dM3 stars (86 targets). We detected rotation in 82 stars (73 dM3 stars, and 9 dM3e stars). We compare our measurements of  $v \sin i$  for all the stars in our dM0, dM2, dM3 and dM4 samples to those from other authors. We find a good agreement down to  $v \sin i$  values of less than  $1 \text{ km s}^{-1}$ . The mean of the differences between measurements is only  $0.42 \text{ km s}^{-1}$ .

We find that the distribution of  $P/\sin i$  for our dM3 stars is different from the distribution of  $P/\sin i$  among our samples of dM2 and dM4 stars. The mean rotation rate for the dM3 stars (excluding dM3e and sdM3 stars) is significantly slower (25.8 days) than for dM2 (14.4 days) and dM4 stars (11.4 days). Analogous behavior also emerges among the faster rotators (dMe stars): we find that a longer rotation period also occurs at spectral sub-type dM3e. Our data suggest that, as regards the rotational properties of lower main sequence stars, spectral sub-type dM3 stands out as exhibiting unusual slow rotation compared to that of adjoining sub-types. Our data lead us to suggest that the unusual rotational properties of M3 dwarfs may represent a signature of the transition to complete convection (TTCC).

*Subject headings:* Stars: late-type dwarfs - Stars: late-type subdwarfs - Stars: rotation

## 1. Introduction

There is a close correlation between stellar rotational period  $P$  and magnetic activity levels in cool dwarfs over a certain range of rotation periods (Soderblom 1982, Vogt et al. 1983, Marcy & Chen 1992, Patten & Simon 1996, Fekel 1997, Delfosse et al. 1998, Jeffries et al. 2000, Pizzolato et al. 2003, Mohanty & Basri 2003). The sense of this "rotation-activity correlation" (RAC) is as follows: the slower a star rotates (i.e. the longer its  $P$ ), the weaker is the level of magnetic activity in that star (other things being equal). Rather than using the period  $P$  alone, it has been found that the Rossby number  $R_0 \sim P/\tau_c$  (where

$\tau_c$  is the convective overturning time) is a useful parameter to quantify the rotation-activity correlation in the case of the X-ray luminosity and the Ca II line core fluxes (e.g. Noyes et al. 1984). The reason why  $R_0$  is particularly useful in quantifying the correlation is that value of  $R_0$  is thought to parameterize how the magnetic dynamo depends on rotation. Although a more recent study by Reiners et al. (2014) suggests that  $L_X/L_{bol}$  correlates better with  $P^{-2}R^{-4}$  (where  $R$  is the stellar radius) than with  $R_0$ , we find it convenient in the present paper to deal with  $R_0$ : the main reason for our choice is that recent efforts to model a dynamo in a deep spherical shell (such as the convective envelopes which exist in M dwarfs) have reported their results as a function of  $R_0$  (Gastine et al. 2012). We shall refer to some of the results from these dynamo models below (Section 7.2).

<sup>1</sup>Based on observations available at Observatoire de Haute Provence and the European Southern Observatory databases and on Hipparcos parallax measurements.

The well-defined RAC mentioned in the above papers extends only over a finite range of periods: when  $P$  becomes shorter than a certain value  $P_c$  (of order several days), the level of activity no longer increases as rapidly with decreasing  $P$ . Instead, for  $P < P_c$ , the activity level tends towards "saturation" (e.g. Walter 1982; Vilhu and Rucinski 1983). In terms of  $R_0$ , saturation is found to set in for numerical values of  $R_0 > 0.1$  (Reiners et al 2009). The onset of saturation at short periods may be associated with nonlinear effects of some kind, or with the existence of a finite upper level of mechanical energy in the convection zone (Mullan 1984), or with a saturation in the field strength which is generated by the dynamo mechanism (Reiners et al 2009; Yadav et al. 2013). Whatever the physical reason(s) for the saturation, it seems likely that, with the reduced sensitivity of activity to rotational period in the saturated regime, the properties of dynamo operation might not be as easy to extract and identify with confidence in that regime (where non-linear effects may dominate) as those properties are in the unsaturated region (where linear behavior may dominate). In the latter region, with  $P$  values longer than a few days, activity levels decrease rapidly as  $P$  becomes longer (varying as  $P^{-4}$  [Walter 1982] in the case of K dwarfs): in these "unsaturated" conditions, the data may contain more readily accessible information about the dynamo properties, and about the processes which lead to rotational braking. For this reason, we focus most of our attention in this paper on "unsaturated" *slowly rotating* M dwarfs, i.e. those with rotational periods which are *longer* than  $P_c$ . As a result of this selection, most of the stars in our sample have low levels of activity.

Only a few previous studies have included slowly rotating field stars (e.g. Marilli et al. 1986, Reiners 2007, Kiraga & Stepien 2007). Houdebine and collaborators (this paper, Papers XV, XVIII, Houdebine et al. 2015) have attempted to measure  $v \sin i$  in slow rotators for a few narrow spectral domains; dK5, dM0, dM2, dM3 and dM4. They successfully measured  $v \sin i$  for a number of stars at these spectral types and derived empirical RAC's.

The principal goal in this paper is the empirical determination of the rotational properties of low mass stars in a range of spectral types extending from dK5 to dM4: within this range, our goal is to present data for certain narrow ranges of sub-types, including dK5, dM0, dM2, dM3, and dM4. A secondary goal is to present a qualitative analysis of our results in terms of

various physical processes which contribute to the loss of angular momentum from stars. One of the physical processes which we consider has to do with the linear size of magnetic loops on M dwarfs, and how these lengths change particularly between M2 and M4 (see Section 7.4).

## 1.1. Stellar rotation: empirical

In this paper, we report on an empirical rotational distribution which we have obtained for a sample of 86 field M dwarfs. The stars in our sample have been chosen specifically to be confined within a narrowly delimited range of spectral sub-types: all of the target stars for which we present data in the present paper are classified as spectral sub-type M3. Our principal goal is to compare and contrast the rotational properties at M3 with those of neighbouring sub-types M2 and M4: in previous papers, rotational data have been published for those neighbouring sub-types.

An independent and extensive study of rotational distributions, including quantitative theoretical modelling of angular momentum loss, has been reported by Reiners and Mohanty (2012: hereafter RM). Stars in the RM study span a much broader range of spectral types than we study here: the RM sample extends from solar type (G2) down to late M. The RM sample also included stars in clusters (with ages up to 650 Myr) as well as field stars (with ages estimated to be on average 3 Gyr). In the present study, by confining our attention to field stars only, we expect that our sample stars are on average older than the oldest cluster reported by RM, i.e. older than 650 Myr.

## 1.2. Stellar rotation: theory

We first make general comments on the loss of angular momentum from a star. Then we summarize the extensive and detailed modelling efforts reported by Reiners and Mohanty (2012: hereafter RM).

### 1.2.1. General

The linear speed  $v_r$  (or angular velocity  $\Omega$ ) with which a star rotates at any particular time in its history is determined by the interplay of a number of factors. (i) The initial conditions which accompanied the formation of the star: the faster the proto-stellar cloud was rotating, the faster the star is likely to be rotating today. (ii) Any variations in the moment of inertia of the star  $I$  (which controls the angular momentum

$J = I\Omega$ ) in the course of evolution will cause reciprocal variations in  $\Omega$  in the absence of torques. (iii) If finite torques are in fact at work (e.g. due to mass loss), then the instantaneous value of  $dJ/dt$  is non-zero. The integrated effects of  $dJ/dt \neq 0$  during the entire course of previous evolutionary time will alter the value of  $J$ , and therefore also the value of  $\Omega$  at any instant of time.

An example of how  $\Omega$  in a particular stellar model (with mass= $1M_{\odot}$ ) varies with time as a result of particular specifications of the various factors can be seen in MacDonald and Mullan (2003: hereafter MM03) (their Fig. 2): from an initial rotation period of 16 days, the model at first speeds up to a rotation period as short as about 1 day at an age of several 10s of Myr, i.e. just as the 1 solar mass star reaches the main sequence. This pre-main-sequence speed-up in rotation is associated with a reduction in  $I$  as the star contracts. Subsequently, during main sequence evolution, the period slows down, reaching periods of 20-30 days at ages of several Gyr. The slowing down on the main sequence is associated with angular momentum loss due to the coupling between a stellar wind and the star's global magnetic field. The latter probably arises from the operation of a dynamo of some kind inside the star.

Further examples of how  $\Omega$  varies with time for stars of various masses can be found in RM (see their Figure 2). One of the RM examples refers to the same mass (1 solar mass) as that modelled by MM03, except that RM chose an initial rotation period of 8 days rather than the 16 days of MM03. The major features reported by MM03 are clearly present in the RM results: there is an initial speed-up in the rotation, which reaches its shortest period at ages of 40-50 Myr, and then the period becomes progressively longer, reaching periods of order 30 days at the present age of the Sun. For stars of lower mass, similar features occur, except that it takes longer for the lower mass stars to reach the main sequence: in the case of the 0.1  $M_{\odot}$  model, the shortest rotation does not occur until an age of 600-700 Myr, which is the time required for such a low mass star to reach the main sequence.

### 1.2.2. *The modeling work of Reiners and Mohanty (RM)*

RM have reported on a modelling study in which they make predictions of rotational periods for low mass stars at various stages of evolution. Their model is based on the following expression for the rate at which the angular momentum  $J$  of a star rotating with

angular velocity  $\Omega$  varies with time due to mass loss:  $dJ/dt = -(2/3) \dot{M} \Omega r_A^2$ . Here,  $\dot{M}$  is the rate of mass loss, and  $r_A$  is the Alfvén radius, i.e. the radial location in the wind where the local wind speed  $v$  equals the local Alfvén speed  $v_A$ . The distance  $D$  out to which the magnetic field of the star is energetically capable of enforcing co-rotation on the wind is equal to  $r_A$ : the distance  $D$  is therefore a measure of the "lever arm" over which the magnetic field can interact strongly enough with the wind to exert torques on the star, thereby braking the star's rotation. The larger  $D$ , the more effective the braking of the star becomes. The numerical value of  $D = r_A$  for any particular star depends on the field strength  $B_o$  on the surface of the star: the latter depends in turn (via some kind of dynamo mechanism) on the angular velocity of the star. RMs approach to modelling  $B_o$  as a function of  $\Omega$  includes two segments: these segments are meant to model the two segments of the RAC mentioned in Section 1 above, i.e. unsaturated at slow rotation, and saturated at fast rotation. To model this, RM assume that at slow rotations ( $\Omega < \Omega_{crit}$ ),  $B_o$  increases with increasing  $\Omega$  according to a power law  $B_o \sim \Omega^a$  (where  $a = 1-2$ ), but at faster rotations ( $\Omega > \Omega_{crit}$ ),  $B_o$  is independent of  $\Omega$ , saturating at a constant value  $B_{crit}$ . (In terms of the discussion in Section 1 above,  $P_c$  and  $\Omega_{crit}$  are related via  $P_c = 2\pi/\Omega_{crit}$ .) Adopting evolutionary tracks from the literature, and assuming that  $v_A$  equals  $K_V v_e(r)$  (i.e.  $v_A$  is proportional to the gravitational escape speed  $v_e$  from the star at  $r_A$ ), RM had most of the ingredients to calculate the evolution of  $J$  for a star of a given mass. For the remaining ingredients, RM adopted a radial field, and assumed that  $\dot{M}$ ,  $B_{crit}$ ,  $\Omega_{crit}$ , and  $K_V$  take on the same numerical values for stars of all masses, and that these numerical values also remain constant with time. RM found that the evolution of  $J$  depends mainly on their choice of numerical values for two quantities:  $\Omega_{crit}$  and a certain constant  $C$ : the latter depends on  $B_{crit}$ ,  $K_V$ , and  $\dot{M}$ .

RM presented empirical data on rotational distributions as a function of both mass and spectral type for various star samples in which the ages were estimated by different methods. E.g. rotation periods of 0.1-10 days were shown for clusters with known evolutionary ages (5 Myr, 130 Myr, and 650 Myr). For older stars, i.e. field stars, the ages of young-disk stars (ages 1-5 Gyr) could be assigned with some confidence based on kinematics. However, the field sample also included some old-disk/halo stars, although RM argued that the presence of such old-disk stars should not skew the re-

sults significantly. The best-fit values  $\Omega_{crit}$  and  $C$  allowed RM to achieve significant success in replicating several crucial (the word used by RM) features of the rotational distributions of stars in clusters at ages of 130 Myr and 650 Myr, as well as for stars in the field. In addition, they were successful in replicating the result reported by West et al (2008) that activity lifetimes increased from  $<1$  Gyr in the earliest M dwarfs to several Gyr in the latest M dwarfs.

### 1.3. Reasons for studying the spectral range dM2-dM4

In this paper, we focus on a much narrower range of spectral types than RM did. The reason we pay particular attention to the spectral sub-types from dM2 to dM4 has to do with the fact that models of M dwarfs on the main sequence are expected to exhibit a transition to complete convection (TTCC) at spectral sub-types M3-M4 (e.g. Mullan and MacDonald 2001). It is believed that stars with a radiative core (including the Sun) have dynamos which are dominated by processes at the interface between the core and the convective envelope. However, in a star which is completely convective, an interface dynamo cannot exist. Therefore, at the TTCC, the dynamo is expected to switch from interface operation to a different regime (e.g. a distributed dynamo). If a change in dynamo regime occurs at the TTCC, perhaps there is also an accompanying change in the angular momentum loss rate  $dJ/dt$ . If we can obtain rotational distributions which are sufficiently detailed, it may be possible to identify a signature of a change in  $dJ/dt$ . The key question in the present paper is: is it possible to narrow down this signature to a specific spectral sub-type?

### 1.4. Summary of the present paper

In the present paper, we do not plan to re-do the evolutionary modeling of RM. Our goal is more restricted: we wish to report on high-precision rotational velocities for a sample of narrowly delimited spectral subtypes. A secondary goal is to analyze the results, in a way which is less detailed than that used by RM.

Our approach is actually consistent with some cautionary remarks made by RM themselves. RM admitted that the number of assumptions and parameters which enter into their formalism is large enough that there is still room for improvement in reaching a quantitative understanding of stellar rotation. They note that Any discrepancies that arise in the compari-

son of our model to the data will motivate an examination of the assumptions *a posteriori*. Among the items listed by RM where they consider that there is room for improvement are the following. (1) The assumption that stars of all masses have the same values of  $\dot{M}$ ,  $B_{crit}$ ,  $\Omega_{crit}$ , and  $K_V$ , and that these values remain unchanged at all evolutionary times. (2) The assumption of purely radial field geometry. (3) The assumption that  $v_A$  scales linearly with  $v_e$ . (4) The numerical values of  $v \sin i$  for M dwarfs are in many cases too small to be reliably measured: as a result, it is hard to determine from the data where exactly the transition from saturation to unsaturation occurs. (5) The magnitude of  $\dot{M}$  in M dwarfs may be quite different from the solar value: RM cite a source which claims that M dwarf stars have  $\dot{M}$  values which are perhaps orders of magnitude larger than the solar value. (6) In the RM theoretical formalism, the mass of the star is used as the primary parameter: however, at the latest spectral types, RM note that different methods of estimating the mass of an M dwarf may differ by up to 30%.

In the present work, we use our own data to address some of these items. E.g., as regards item (2), we examine (in Section 7.3 and 7.4) the non-radial properties of fields in M dwarfs. As regards item (3), we examine (in Section 7.1) a possible rationale for how the Alfvén radius might vary from one M dwarf to another. As regards item (4), a principal goal of the present work (Section 4) is to report on  $v \sin i$  values which push beyond the limits of detectability which had constrained some of the RM data, thereby providing a better chance to possibly detect the transition from saturated to unsaturated dynamo behaviour. As regards item (5), we consider (in Section 7.1) some evidence which suggests that  $\dot{M}$  in M dwarfs may be smaller than the solar value. As regards item (6), we prefer to use colors and spectral types (rather than masses) to identify which stars should be included in our sample: these are immediately accessible to observation (Section 2), and our data sets do not rely on knowing the mass of any star in the sample. As regards item (1), our approach can make no comment.

In this paper, we report on empirical rotational distributions which have been obtained for field stars at spectral sub-type M3. With field stars, we expect that our sample stars are significantly older than the oldest cluster reported by RM, i.e. older than 650 Myr. The stars which are of most interest to us (at spectral type M3), arrive on the main sequence (MS) at ages of 200 Myr (see RM). By confining attention to stars with

ages older than 650 Myr, our sample stars would have reached the main sequence long ago. To the extent that this is valid, it is meaningful for us to consider testing the theoretical prediction that on the main sequence, stars become fully convective at spectral types in the vicinity of M3.

## 2. Observations

### 2.1. Selection of our sample stars

In previous studies (e.g. Houdebine & Stempels 1997 Paper VI, Houdebine 2008 Paper VII, Papers XV, XVIII) we have chosen to isolate samples of stars according to their effective temperatures, i.e. based on photospheric conditions. This photospheric emphasis was shown to be necessary even when we were interested in modelling chromospheres in M dwarfs: we found that the formation of chromospheric lines depends on the photospheric conditions as indicated by  $T_{eff}$ . At first sight, this may seem somewhat paradoxical, but in support of this claim, we offer the following.

If we were studying specifically stars which had highly active chromospheres, then it would be true that the formation of chromospheric lines would be dominated by the way in which mechanical energy deposition controls local conditions in the chromosphere. In such stars, the Balmer lines are strongly in emission. However, in choosing our sample of stars, we have *not* relied on selecting stars with high activity (see Section 2.2 below). In fact the opposite is true. The sample includes a significant number of stars which were included in the HARPS archives because they had been observed specifically in order to search for exoplanets. In such searches, the presence of a high level of magnetic activity is typically used to exclude stars from the exoplanet sample: variability associated with activity can obscure the variability associated with a putative planet motion. As a result, there could be a bias in our sample towards stars with low levels of activity. This has an important consequence in the context of an early M dwarf: in such a star, the photosphere generates Balmer lines which are weakly in absorption. But if a low level of mechanical flux is deposited in the atmosphere of such a star, models predicted a result which is somewhat surprising: the effect is not to generate Balmer lines in emission. On the contrary, the effect is to drive the Balmer lines more strongly into absorption (Cram & Mullan 1979, Houdebine & Stempels 1997). The equivalent width of  $H_\alpha$  in absorption reaches a maximum value (about 0.7 Å in an M0 star)

at a certain flux of mechanical energy. Subsequent increases in mechanical flux result at first in filling in the absorption. Eventually, when the mechanical energy flux exceeds a critical value, the Balmer lines do indeed go into emission. These predictions were verified by Stauffer and Hartmann (1986) in their observations of about 200 M dwarfs in the Gliese catalog. Thus, in M dwarfs with low activity levels, such as many of the stars in the HARPS exoplanet archive, the Balmer spectrum retains the absorption characteristic which is most often associated with the photosphere. The study of the effect of the effective temperature on the H I and Ca II spectral lines can also be found in Houdebine & Doyle (1994) for spectral types from G to M.

As regards the current study of the rotation of M dwarfs, the photospheric conditions once again play an important role: indeed we showed in previous studies (Paper VII, Houdebine 2010b Paper XIV, Houdebine 2011b Paper XVI, Houdebine 2012 Paper XVII, Houdebine et al. 2015) as well as in the present study that the rotation properties of M dwarfs depend on the effective temperature (which correlates with radius and mass, Kiraga & Stepień 2007). Therefore, it is crucial if one wants to investigate the rotation in M dwarfs to isolate stellar samples with the same effective temperature and not intermingle multiple spectral types such as in Nielsen et al. (2013). In order to isolate a sample of dM3 stars with the same effective temperature, we decided to select our stars according to their R-I colour. We showed in previous papers (cited above) that this colour is a good effective temperature indicator and has relatively low sensitivity to metallicity. Moreover R-I data are widely available for nearby stars and have a high precision.

All the stars in our selected sample have similar R-I colours (see Table 1), and the same effective temperature of 3290 K to within  $\pm 60$  K with only a few exceptions. Our choice of R-I colours corresponds approximately to the spectral type dM3 (Leggett 1992). We note, however, that spectral classification may differ from one author to another. In this regard, in previous Papers on dM1 stars (Paper VII, XII, Houdebine 2009b Paper XIII, Paper IX, Paper XIV, Houdebine 2010c Paper X, Paper XV, Houdebine et al. 2012 Paper XIX), we used a different calibration. According to their infrared colours and the classification of Leggett (1992) these stars are in fact dM2 stars. We shall use in the future this calibration and therefore all our previous work on "dM1" stars in this series of papers should be considered as papers referring to dM2 stars.

We selected stars with  $(R-I)_c$  (R-I in the Cousins system) in the range [1.284;1.416] with a few exceptions close to this range, which also corresponds to  $(R-I)_K$  (R-I in the Kron system) in the range [1.003;1.113] according to the transformation formulae of Leggett (1992) (see Leggett 1992 for more information on the Cousins’s and Kron photometric systems). Values of  $(R-I)$  were taken from the following papers: Veeder (1974), Eggen (1974), Rodgers & Eggen (1974), Eggen (1976a, 1976b), Eggen (1978), Eggen (1979), Eggen (1980), Weis & Uppgren (1982), Uppgren & Lu (1986), Eggen (1987), Booth et al. (1988), Leggett & Hawkins (1988), Bessel (1990), Weis (1991a 1991b), Dawson & Forbes (1992), Leggett (1992), Weis (1993).

We selected a list of 381 dM3 stars from measurements of R-I in the literature. We searched the European Southern Observatory (ESO) and Observatoire de Haute Provence (OHP) databases for spectroscopic échelle observations of these stars. In these databases, we found observations for 86 distinct dM3 stars from two different échelle spectrographs; HARPS (High Accuracy Radial velocity Planet Search, ESO) and SOPHIE (OHP).

## 2.2. Biases in our sample stars

The stars in our sample include all of the dM3 stars which are present in the databases from all observing programs with HARPS and SOPHIE. These programs are for the most part planet-search programs, but they also include some programs on magnetic activity. Our sample of stars is brightness limited: as such, there is a bias towards the brighter M dwarfs, i.e., towards stars within the spectral subtype M3 with closer distances and/or larger radii.

We find that our initial target list is complete to a visual magnitude of 13.5. This corresponds to an absolute magnitude of 11.45 (the limit from normal dwarfs to subdwarfs) at a distance of 26 pc for main-sequence disk stars. For halo stars (M3 subdwarfs) the target list is complete only to a much smaller distance because of the intrinsic faintness of these objects. We find that among our target list, all dM3 stars of visual magnitude  $\sim 12$  or brighter have been observed and are in the present sample of stars. For an absolute magnitude of 11.45, this implies a maximum distance of 13 pc. Therefore, we believe that our stellar sample is complete for old disk and young disk stars out to a distance of about 13 pc.

As far as the bias towards bright stars is concerned, we found it has little effects on the mean rotation period of low activity dM3 stars (see Sect. 6). This is due to the fact that the rotation period does not change much with the stellar radius for disk stars (see Sect. 6). For the same reason, this bias, although important, has little consequences on the RAC. We emphasize here that our calculated mean rotation periods (reported below in Section 6) refer to disk stars only. We do not include M3 subdwarfs.

In the planet-search programs in the HARPS and SOPHIE databases, the observers tend to avoid very active stars because their spot modulation mimic the effects of planets and adds considerably to noise in the data. Therefore our stellar sample is biased towards low activity stars. However, we found that some 10is enhanced to some extent compared to the dM3 stars. The important point is that all M3 dwarfs brighter than  $m_v=12$  seem to have been observed, and our sample is somewhat biased towards low activity stars.

As far as other spectral types are concerned (dK5, dM0, dM2 and dM4), we rely on the same properties of the rotation period as a function of radius (Houdebine 2010, Paper XIV, Houdebine 2011, Paper XVI, Houdebine 2012, Paper XVII). Therefore, for all these spectral types we do not expect the bright star bias to present a problem in determining the mean rotation period of slow rotators. Also, for all these spectral types except the dM0 spectral type, the sample includes up to about 10 rotation-activity relationships which we derive should be reliably inter-comparable among the various subtypes. We have only a slight problem with dM0 stars, because the sampling of active stars includes only one dM0(e) star and one dM0e star. Therefore the rotation-activity relationship is not as well defined at high activity levels for this spectral type (see Houdebine et al. 2015). Nevertheless, this has no significant effect on the conclusions of the present study.

We emphasize that for all stars in our subsamples from dM2 to dM4, we have used the same relationship between R-I color and effective temperature, and the same relationship between absolute magnitude and radius (see Section 3 below). As a result, even if there may be uncertainties in the individual numerical values of  $T_{eff}$  and radius which we derive from these relationships, nevertheless, in a *differential* study involving a comparison between stars of various subtypes from dK5 to dM4, the relative uncertainties should be much smaller. It is precisely such a differential study

that leads to the result which we regard as among the most significant in the present paper (see Fig. 10 below).

### 2.3. Spectrographs and data reduction

The two high-resolution échelle spectrographs whose data are used in the present paper were intended for planet search programs and were designed to be extremely stable in wavelength and resolution. This stability makes them well suited for the measurement of rotational velocities in slowly rotating M dwarfs.

HARPS is a fiber-fed high resolution echelle spectrograph mounted on the 3.6m telescope at ESO-La Silla Observatory. HARPS is the ESO facility for the measurement of radial velocities with the highest precision currently available (about  $0.001 \text{ km s}^{-1}$ ). In order to achieve this goal, this spectrograph is fed by a pair of fibers and is optimized for mechanical stability. It is contained in a vacuum vessel to avoid spectral drift due to air temperature and pressure variations. The resolving power of HARPS is 115,000. The spectral range covered is 378-691 nm. An automated reduction procedure reduces the spectra collected and yields a precise radial velocity. A more complete description of this spectrograph can be found in Mayor et al. (2003).

SOPHIE is a cross-dispersed echelle spectrograph located in a temperature-controlled room at OHP. The spectra cover the wavelength range 387-694 nm. The instrument is computer controlled and a standard data reduction pipeline automatically reduces the data upon CCD readout. The spectrograph resolution is 75,000, and the precision in radial velocities is  $0.002\text{-}0.003 \text{ km s}^{-1}$  which makes it one of the most stable spectrographs in the world. A more complete description of this spectrograph can be found in Perruchot et al. (2008).

### 3. Stellar parameters

The methods we use to derive the effective temperature and the stellar radius for each star are the same as in our previous studies on M dwarfs. In order to derive effective temperatures ( $T_{eff}$ ) for dM3 stars, we used the calibration of Jones et al. (1994) for M dwarfs. We used the formulae:

$$T_{eff} = -799 \times (R - I)_c + 4372K \quad (1)$$

This relation is valid down to  $(R-I)_c=2.3$ . Jones et al.

(1994) quote a precision of  $\pm 50 \text{ K}$  on their temperature determinations.

In order to derive the stellar radii, we used the classical formula;

$$M_v + BC = 42.36 - 5 \times \log \frac{R}{R_\odot} - 10 \times \log T_{eff}, \quad (2)$$

where symbols take their usual meaning. The value of BC varies with stellar temperature. We used the BC tabulation with  $(R-I)_c$  from Kenyon & Hartmann (1995) in order to calculate BC. The stellar radii and the effective temperatures are listed in Table 1 for all our target stars.

Table 1: Parameters of dM3 stars in our sample, including the  $S/N$  ratio for the sum of the spectra for each star, as well as the number of spectra. The full table is available from the authors upon request.

Star	$v$ (mag)	$(R-I)_c$ (mag)	Teff (K)	Spectral Type	$\pi$ ( $m''$ )	Distance (pc)	Mv (mag)	$R_*$ ( $R_\odot$ )	No.of spec.	S/N HARPS @5000Å	S/N SOPHIE @5000Å
GJ 1046	11.595	1.292	3350 $\pm$ 50	dM3	71.06 $\pm$ 3.23	14.07	10.85 $\pm$ 0.09	0.426 $\pm$ 0.029	6	61	-
GJ 1050	11.730	1.322	3320 $\pm$ 50	dM3	66 $\pm$ 13	15.2	10.83 $\pm$ 0.39	0.450 $\pm$ 0.085	9	69	-
GJ 1097	11.456	1.400	3250 $\pm$ 50	dM3	81.38 $\pm$ 2.49	12.29	11.01 $\pm$ 0.06	0.461 $\pm$ 0.026	7	71	-
GJ 1125	11.710	1.125	3470 $\pm$ 50	sdM3	103.46 $\pm$ 3.94	9.67	11.78 $\pm$ 0.09	0.224 $\pm$ 0.015	8,5,3	68	63HR,62HE
GJ 1203	12.158	1.352	3290 $\pm$ 50	dM3	59.63 $\pm$ 3.55	16.77	11.04 $\pm$ 0.12	0.425 $\pm$ 0.035	8	44	-
GJ 1212A	12.032	1.403	3250 $\pm$ 50	dM3	53.41 $\pm$ 4.76	18.72	11.42 $\pm$ 0.19	0.383 $\pm$ 0.043	1	10	-
GJ 1212B	12.032	1.403	3250 $\pm$ 50	dM3	53.41 $\pm$ 4.76	18.72	11.42 $\pm$ 0.19	0.383 $\pm$ 0.043	1	10	-
GJ 1271	11.704	1.298	3340 $\pm$ 50	dM3	47.52 $\pm$ 2.82	21.04	10.09 $\pm$ 0.12	0.612 $\pm$ 0.049	4,4	-	61HR,79HE
GJ 2121	12.280	1.386	3270 $\pm$ 50	dM3	44.58 $\pm$ 5.36	22.43	10.53 $\pm$ 0.24	0.563 $\pm$ 0.074	1	8	-
GJ 3139	11.770	1.333	3310 $\pm$ 50	dM3	50.68 $\pm$ 2.53	19.73	10.29 $\pm$ 0.11	0.585 $\pm$ 0.045	2	29	-
GJ 3160A	12.01	1.292	3340 $\pm$ 50	dM3	38.45 $\pm$ 3.15	26.01	10.69 $\pm$ 0.18	0.461 $\pm$ 0.049	1	10	-
GJ 3160B	12.01	1.292	3340 $\pm$ 50	dM3	38.45 $\pm$ 3.15	26.01	10.69 $\pm$ 0.18	0.461 $\pm$ 0.049	1	10	-
GJ 3189	12.67	1.318	3320 $\pm$ 50	sdM3	95.5 $\pm$ 10.9	10.5	12.57 $\pm$ 0.23	0.201 $\pm$ 0.026	9	42	-
GJ 3279	11.8	1.324	3310 $\pm$ 50	dM3	65 $\pm$ 13	15	10.86 $\pm$ 0.40	0.445 $\pm$ 0.086	10	69	-
GJ 3293	12.0	1.308	3330 $\pm$ 50	dM3	55 $\pm$ 9	18	10.70 $\pm$ 0.33	0.469 $\pm$ 0.078	19	89	-
GJ 3404A	11.73	1.412	3250 $\pm$ 50	dM3	64 $\pm$ 9	16	10.76 $\pm$ 0.29	0.525 $\pm$ 0.079	19	102	-
GJ 3412A	11.028	1.393	3260 $\pm$ 50	sdM3	95.43 $\pm$ 2.36	10.48	11.68 $\pm$ 0.05	0.335 $\pm$ 0.017	1	-	41HR
GJ 3412B	11.028	1.393	3260 $\pm$ 50	sdM3	95.43 $\pm$ 2.36	10.48	11.68 $\pm$ 0.05	0.335 $\pm$ 0.017	1	-	41HR
GJ 3459	11.712	1.390	3260 $\pm$ 50	sdM3	94.31 $\pm$ 3.31	10.60	11.58 $\pm$ 0.08	0.349 $\pm$ 0.022	7	63	-
GJ 3528	11.728	1.300	3330 $\pm$ 50	dM3	51.25 $\pm$ 3.72	19.51	10.28 $\pm$ 0.15	0.563 $\pm$ 0.053	6	59	-
GJ 3563	11.953	1.311	3330 $\pm$ 50	dM3	63.47 $\pm$ 3.54	15.76	10.97 $\pm$ 0.11	0.415 $\pm$ 0.032	11	66	-
GJ 3598	12.46	1.292	3340 $\pm$ 50	dM3	45 $\pm$ 9	22	10.73 $\pm$ 0.39	0.452 $\pm$ 0.085	1	7	-
GJ 3634	11.95	1.291	3340 $\pm$ 50	dM3	56 $\pm$ 11	18	10.69 $\pm$ 0.39	0.460 $\pm$ 0.087	49	145	-
GJ 3643	12.369	1.346	3300 $\pm$ 50	dM3	50.90 $\pm$ 4.58	19.65	10.90 $\pm$ 0.19	0.450 $\pm$ 0.050	1	8	-
GJ 3708A	11.709	1.376	3270 $\pm$ 50	dM3	79.43 $\pm$ 2.36	12.59	11.21 $\pm$ 0.06	0.406 $\pm$ 0.023	8	63	-
GJ 3846	12.257	1.399	3250 $\pm$ 50	sdM3	70.03 $\pm$ 4.89	14.28	11.48 $\pm$ 0.15	0.371 $\pm$ 0.036	6	44	-
GJ 3892	11.473	1.340	3300 $\pm$ 50	dM3	69.19 $\pm$ 2.60	14.45	10.67 $\pm$ 0.08	0.496 $\pm$ 0.032	8	74	-
GJ 3916A	11.279	1.306	3330 $\pm$ 50	dM3	66.21 $\pm$ 3.18	15.10	11.13 $\pm$ 0.11	0.383 $\pm$ 0.029	3	42	-
GJ 3916B	11.279	1.306	3330 $\pm$ 50	dM3	66.21 $\pm$ 3.18	15.10	11.13 $\pm$ 0.11	0.383 $\pm$ 0.029	3	42	-
GJ 4004	12.1	1.455	3210 $\pm$ 50	sdM3	81 $\pm$ 16	12	11.64 $\pm$ 0.39	0.373 $\pm$ 0.071	2	28	-
GJ 4129	11.95	1.304	3330 $\pm$ 50	dM3	63.1 $\pm$ 3.8	15.8	10.95 $\pm$ 0.13	0.416 $\pm$ 0.036	1	11	-
Gl 12	12.61	1.415	3240 $\pm$ 50	sdM3	84 $\pm$ 11	12	12.23 $\pm$ 0.27	0.268 $\pm$ 0.038	6,2	37	37HE
Gl 70	10.915	1.274	3350 $\pm$ 50	dM3	87.62 $\pm$ 2.00	11.41	10.63 $\pm$ 0.05	0.463 $\pm$ 0.024	7,7	98	105HR



Table 2: Results for  $v \sin i$  and  $P/\sin i$  for M3 stars, including standard deviations. We put in parenthesis the detections below  $3\sigma$ . Also listed: FWHMs of the cross-correlation line profiles. The full table is available from the authors upon request.

Star	FWHM ( $\text{\AA}\pm$ ) HARPS	FWHM ( $\text{\AA}\pm$ ) SOPHIE	$v \sin i \pm \sigma$ ( $\text{km s}^{-1}$ ) HARPS	$v \sin i \pm \sigma$ ( $\text{km s}^{-1}$ ) SOPHIE	Mean $v \sin i$ ( $\text{km s}^{-1}$ )	$P/\sin i \pm \sigma$ (days)
GJ 1046	0.1273 0.0011	-	2.63±0.064	-	2.63	8.20±0.76
GJ 1050	0.1063 0.0011	-	(0.59+0.26-0.52)	-	0.59	(38.4-17+40)
GJ 1097	0.10505 0.0011	-	0.00	-	<0.5	>47
GJ 1125	0.1063 0.0011	0.1401 0.0014	(0.59+0.26-0.52)	1.39+0.20-0.24	0.99	(11.5-1.5+2.4)
GJ 1203	0.1072 0.0011	-	(0.82+0.29-0.18)	-	0.82	(26.2-6.5+18)
GJ 1212A	0.1066 0.0011	-	(0.69+0.22-0.44)	-	0.69	(28.1-9.2+40)
GJ 1212B	0.1077 0.0011	-	(0.90+0.16-0.22)	-	0.90	(22.0-5.2+9.9)
GJ 1271	-	0.1401 0.0014	-	1.39+0.20-0.24	1.39	22.3-4.4+6.8
GJ 2121	0.1187 0.0011	-	2.06+0.08-0.18	-	2.06	13.9-2.3+3.3
GJ 3139	0.1077 0.0011	-	(0.90+0.16-0.22)	-	0.90	(32.8-7.0+14)
GJ 3160A	0.1080 0.0011	-	0.95+0.15-0.18	-	0.95	24.5-5.5+9.0
GJ 3160B	0.1088 0.0011	-	1.06+0.14-0.16	-	1.06	22.0-4.6+6.6
GJ 3189	0.1125 0.0011	-	1.42±0.09	-	1.42	7.18±1.2
GJ 3279	0.1074 0.0011	-	(0.85+0.17-0.26)	-	0.85	(26.4-8.6+19)
GJ 3293	0.1074 0.0011	-	(0.85+0.17-0.26)	-	0.85	(27.9-8.5+19)
GJ 3404A	0.1077 0.0011	-	(0.90+0.16-0.22)	-	0.90	(29.5-8.2+15)
GJ 3412A	-	0.135 0.0034	-	<0.5	<0.5	-
GJ 3412B	-	0.134 0.0034	-	<0.5	<0.5	-
GJ 3459	0.1066 0.0011	-	(0.69+0.22-0.44)	-	0.69	(25.7-7.4+40)
GJ 3528	0.1077 0.0011	-	(0.90+0.16-0.22)	-	0.90	(31.7-7.2+14)
GJ 3563	0.1074 0.0011	-	(0.85+0.17-0.26)	-	0.85	(24.7-5.7+13)
GJ 3598	0.1066 0.0011	-	(0.69+0.22-0.44)	-	0.69	(33.2-13+40)
GJ 3634	0.1074 0.0011	-	(0.85+0.17-0.26)	-	0.85	(27.3-8.8+19)
GJ 3643	0.1083 0.0011	-	1.00+0.14-0.18	-	1.00	22.8-5.0+8.1
GJ 3708A	0.1060 0.0011	-	(0.50+0.30-0.50)	-	0.50	(41.1-17+40)
GJ 3846	0.1072 0.0011	-	(0.82+0.18-0.29)	-	0.82	(22.9-5.9+16)
GJ 3892	0.1072 0.0011	-	(0.82+0.18-0.29)	-	0.82	(30.7-7.1+19)
GJ 3916A	0.1102 0.0011	-	1.24±0.14	-	1.24	15.6-2.6+3.3
GJ 3916B	0.1447 0.0011	-	3.51±0.05	-	3.51	5.52±0.50
GJ 4004	0.1063 0.0011	-	(0.59+0.26-0.52)	-	0.59	(32.0-14+40)
GJ 4129	0.1060 0.0011	-	(0.50+0.30-0.50)	-	0.50	(42.0-18+40)
Gl 12	0.1080 0.0011	-	0.95+0.15-0.18	-	0.95	14.2-3.6+5.9
Gl 70	0.1074 0.0011	0.1388 0.0014	(0.85+0.17-0.26)	(1.17+0.24-0.26)	1.01	(23.2-4.3+7.0)
Gl 109	-	0.1398 0.0014	-	1.34+0.22-0.24	1.34	15.6-2.8+4.3
Gl 145	0.1074 0.0011	-	(0.85+0.17-0.26)	-	0.85	(22.0-4.6+11)
Gl 163	0.1074 0.0011	-	(0.85+0.17-0.26)	-	0.85	(29.1-6.2+15)
Gl 204.2	0.1066 0.0011	-	(0.69+0.22-0.44)	-	0.69	(40.2-13+40)
Gl 207.1	0.3141 0.0011	0.3318 0.0014	9.27±0.034	9.77±0.05	9.52	2.81±0.25
Gl 226	-	0.1385 0.0014	-	(1.12+0.24-0.27)	1.12	(21.8-4.6+8.3)
Gl 238	0.1074 0.0011	-	(0.85+0.17-0.26)	-	0.85	(31.4-6.7+16)
Gl 251	-	0.1386 0.0014	-	(1.14+0.24-0.27)	1.14	(18.9-3.9+6.8)
GL 298	0.1083 0.0011	-	1.00+0.14-0.18	-	1.00	27.4-5.0+8.3
GL 352	0.1527 0.0011	-	3.89±0.05	-	3.89	8.51±0.65
Gl 357	0.1077 0.0011	-	(0.90+0.16-0.22)	-	0.90	(20.8-3.9+7.8)
Gl 358	0.1100 0.0011	-	1.21±0.14	-	1.21	19.8-2.9+3.6

#### 4. Determination of the projected rotation periods

In this paper, we use the same technique as in previous studies in order to determine the projected rotational broadening  $v \sin i$ : we use a cross-correlation technique for a selected narrow spectral range. The choice of the spectral range is crucial in order to obtain cross-correlation profiles that are as clean as possible, as well as having low background noise (see also Sect. 5). For dM3 stars, we used a  $150\text{\AA}$  wide spectral domain in the red end of the spectrum, between  $6650\text{\AA}$  and  $6800\text{\AA}$  (see Fig. 1, which shows the spectrum of one particular star in our dM3 sample: G1 436). In this wavelength range, the presence of many weak and unsaturated narrow spectral lines yield clean cross-correlation functions as well as a low background noise. We have found that the spectral lines in the red yield the best cross-correlation results for dM2, dM3 and dM4 stars.

Because our stars all have closely similar spectral types, it is possible to intercompare the spectra and look for possible rotational broadening effects with the highest precision. The broadening of the lines depend on three main parameters; rotational broadening, and

micro- and macro- turbulence. The latter parameters (probably associated in some way with the turbulent motions of convectively rising/falling gas, and with numerical values of typically  $1\text{ km/s}$ ) are not expected to vary much among our narrowly selected sample of dM3 stars. Metallicity plays a role in the strengths of the lines, but less significantly in their shapes. Therefore, changes in spectral line widths from one star to another are expected to depend mainly on differences in rotational velocity from star to star.

The procedure of selecting appropriate templates for low  $v \sin i$  values is the same as in previous papers. We found that the best template for HARPS is GJ 1097 with FWHM of only  $0.10505\text{\AA}$  ( $4.69\text{ km/s}$ ). This is broader than the  $0.1006\text{\AA}$  FWHM ( $5.46\text{ km/s}$ ) we measured for dM2 stars. However this increased broadening is consistent with the different wavelength domains we used in calculating the cross-correlations (for dM2 stars we used the wavelength range  $5460\text{\AA} - 5585\text{\AA}$ ). For SOPHIE, we found that the best template is G1 655 with a FWHM of the cross-correlation peak of  $0.1349\text{\AA}$ .

In order to measure  $v \sin i$ , we cross-correlated the stellar spectra with the template spectrum. We then subtracted the cross-correlation background following the same method as in Paper XIV. We then measured the FWHM of the cross-correlation peaks. In order to recover  $v \sin i$  from the FWHM we then proceeded as follows: We computed the theoretical rotational profiles including limb darkening for the following series of  $v \sin i$  values (in units of  $\text{km s}^{-1}$ ): 0.00, 0.025, 0.25, 0.50, 0.75, 1.00, 1.50, 2.00, 2.50, 3.00, 4.0, 5.0, 7.0, 10.0 and 15.0. We then convolved the theoretical rotational profiles with the cross-correlation profile of GJ 1097 for HARPS and G1 655 for SOPHIE. We measured the FWHM of the convolved theoretical rotational profiles and show these measurements as a function of  $v \sin i$  in Fig. 2 for HARPS and SOPHIE. We use this diagram to derive  $v \sin i$  values from our calculated FWHM result for each star. The measured FWHM,  $v \sin i$ , and  $P/\sin i$  values are listed in Table 2. The values in parenthesis are possible values but with a large uncertainty (see next Section).

We found that non-zero values for  $v \sin i$  could be obtained for most of our dM3 stars; the values of  $v \sin i$  were found to be typically in the range  $0.5\text{--}2\text{ km s}^{-1}$ . The  $v \sin i$  values are smaller on average for dM3 stars than for dM2 and dM4 stars. We find that on average,  $v \sin i = 1.05\text{ km s}^{-1}$  for dM3 stars (excluding spectroscopic binaries, sdM3 and dM3e stars),

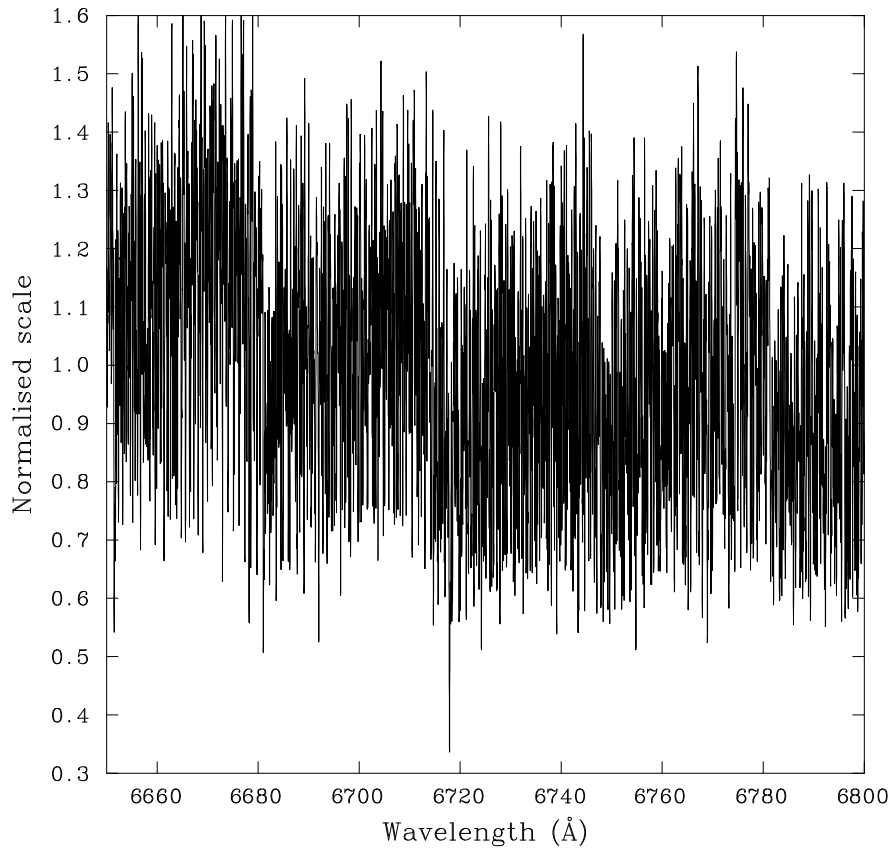


Fig. 1.— The spectral range  $6650\text{\AA}$  -  $6800\text{\AA}$  used for our cross-correlations for the star Gl 436: this range yields very clean cross-correlation profiles at sub-type dM3. The  $S/N$  ratio for Gl 436 is about 800 in this range. The variations relative to the continuum are not noise: they are due to numerous blended weak absorption lines. The mean flux in this spectrum has been normalised to 1 for clarity.

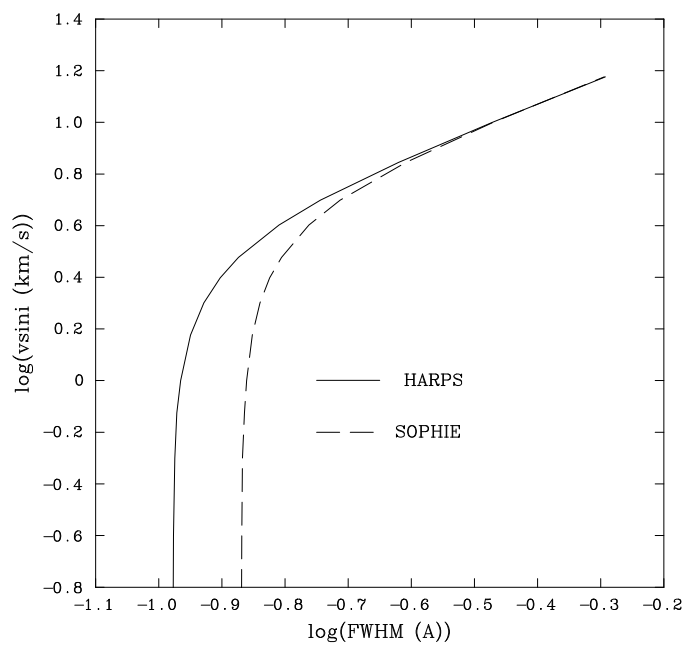


Fig. 2.— Plots of the conversion between the measured FWHM (in Å) of the cross-correlation peaks and the numerical value of  $v \sin i$ . Solid line: HARPS data. Dashed line: SOPHIE data.

whereas we found  $v \sin i = 2.41 \text{ km s}^{-1}$  for dM2 stars and  $v \sin i = 1.57 \text{ km s}^{-1}$  for dM4 stars. As we shall see below (Fig. 6), this also implies longer rotation periods for dM3 stars than for dM2 and dM4 stars.

With HARPS, we also observed a few stars of particular interest; six spectroscopic binaries (GJ 1212AB, GJ 3160AB, GJ 3412AB, GJ 3916AB, Gl 644AB, Gl 735AB). For five of these stars, the components are well separated. For GJ 3412AB (observed with SOPHIE), the two components are blended. In this case we applied multi-Gaussian fits to the cross-correlation profile.

## 5. Sources of uncertainty in our $v \sin i$ values

### 5.1. Uncertainties due to the background

In Houdebine (2010b), using four different spectrographs and comparing our results with those of other authors, we showed that we could attain a detection limit of  $1 \text{ km s}^{-1}$  and a precision of  $0.3 \text{ km s}^{-1}$  for dM2 stars. Here, for dM3 stars the situation is very similar, except that we have even lower background noise in the cross-correlation functions than for dM2 stars. To illustrate this, we show the cross-correlation functions for three stars in Fig. 3: GJ 4129 ( $v \sin i = 0.50 \text{ km s}^{-1}$ ), Gl 581 ( $v \sin i = 0.50 \text{ km s}^{-1}$ , a subdwarf), and Gl 781.1A ( $v \sin i = 0.25 \text{ km s}^{-1}$ ). One can see in this diagram that the cross-correlation peaks for the three stars are very similar to one another, because of their low  $v \sin i$ . This is an indication of the excellent stability of the spectrographs we use. On the other hand, one can also note that there are small variations from star to star in the cross-correlation background. We estimate that the amplitude of these variations are about 2% ( $3\sigma$ ) of the intensity of the cross-correlation peaks. We found that this uncertainty on the background yields an uncertainty of  $3\sigma = 0.0034 \text{ \AA}$  on the FWHM for HARPS, and  $3\sigma = 0.0042 \text{ \AA}$  on the FWHM for SOPHIE. Therefore our measurements for dM3 stars are even more precise than those for dM2 stars. Moreover, these figures are estimates due to the noise in the background. But the S/N ratio in the cross-correlation peaks themselves is higher (several hundred). If our measurements were incorrect we would not obtain such good correlations: instead we would obtain scatter diagrams. Further confirmation that our measurements are not incorrect is provided by the continuity in the gradients of the RAC's which are found to increase continuously from our dK5 sample to our dM4 sample (Houdebine et al. 2015).

As one can see from Fig. 2, the uncertainty of  $3\sigma = 0.0034 \text{ \AA}$  on the FWHM yields a variable uncertainty on  $v \sin i$  depending on its magnitude. Indeed, because the curves in Fig. 2 are increasingly steep at small  $v \sin i$ , the uncertainty in  $v \sin i$  increases at low values of  $v \sin i$ . We quantify these uncertainties ( $\pm\sigma$ ) on  $v \sin i$  for each measurement for HARPS and SOPHIE and list the results in Table 2. If we take into account the limits of  $\pm 3\sigma$  given above, the value of  $v \sin i$  cannot be reliably measured below  $0.95 \text{ km s}^{-1}$  for HARPS. The corresponding figure is  $1.22 \text{ km s}^{-1}$  for SOPHIE. The width of the template cross-correlation function is only  $4.61 \text{ km s}^{-1}$  for HARPS. A  $1 \text{ km s}^{-1}$  broadening corresponds to a broadening of the cross-correlation function of 3%. We show the results of our convolved cross-correlations in Fig. 4 for values of  $v \sin i$  of 0.0 (GJ 1097), 0.5, 1.0, 1.5, 2.0, 2.5, 3.0, 4.0, 5.0, 7.0, 10.0 and  $15.0 \text{ km s}^{-1}$  for HARPS. We obtain our simulations of rotational broadening of our cross-correlation profiles by convolving them with our rotational profiles. We find that we can measure  $v \sin i$  values down to  $250 \text{ m s}^{-1}$ . Inspection of Fig. 4 shows that one can easily differentiate the template profile (leftmost curve) from the profile which has been broadened by  $1.0 \text{ km s}^{-1}$  (shown as the third curve in from the leftmost curve). This confirms our previous findings that our cross-correlation technique enables us to evaluate  $v \sin i$  readily down to values as small as  $1.0 \text{ km s}^{-1}$ . Further observations in the future with higher spectral resolution spectrographs such as ESPRESSO (Echelle SPectrograph for Rocky Exoplanet and Stable Spectroscopic Observations, ESO, R=220,000) could confirm our measurements below our  $3\sigma$  detection limit.

### 5.2. Gaussian profiles versus rotational profiles

We also convolved our template cross-correlation profile for HARPS (GJ 1097) with Gaussians in which the broadenings were set equal to those of our theoretical rotational profiles (as listed above). Once again, we found that we could distinguish rotational broadening for  $v \sin i$  as low as  $250 \text{ m s}^{-1}$ . However, we found that in general the broadened profiles using Gaussians are narrower than those broadened with our rotational profiles taking into account limb-darkening effects. To illustrate this, we show in Fig. 5 the FWHM of our Gaussian broadened profiles as a function of the FWHM of our profiles broadened when taking into account limb-darkening. One can see that the Gaussian broadened profiles are narrower than the profiles that account for limb-darkening. There

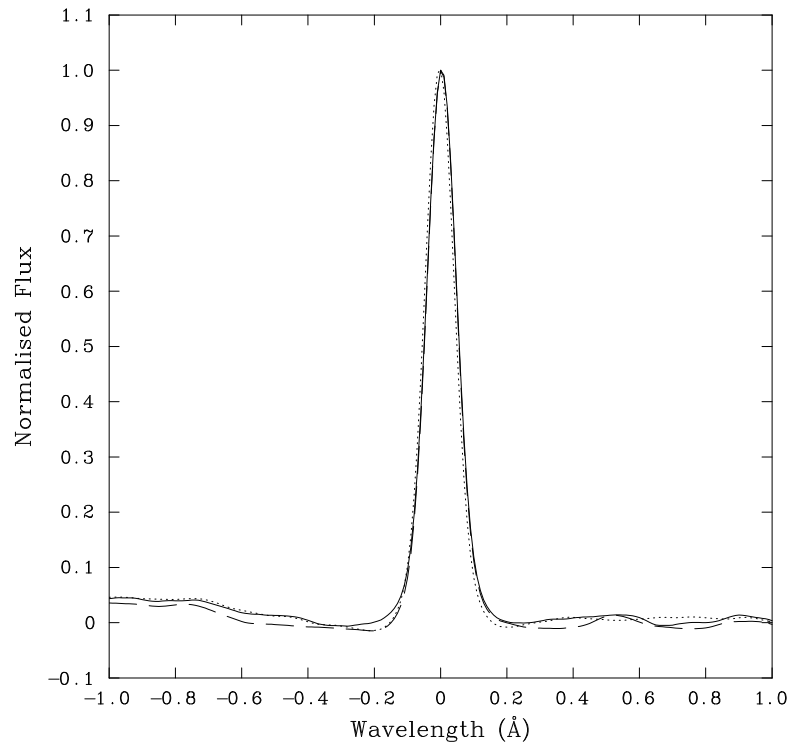


Fig. 3.— Cross-correlation functions derived for GJ 4129 ( $v \sin i = 0.50 \text{ km s}^{-1}$ , continuous line), GJ 581 ( $v \sin i = 0.50 \text{ km s}^{-1}$ , dashed line) and GJ 781.1A ( $v \sin i = 0.25 \text{ km s}^{-1}$ , dotted line) with GJ 1097, corrected for the background in GJ 1097. The major source of uncertainty in our measurements of  $v \sin i$  is caused by the (small) fluctuations in the background from one star to another.

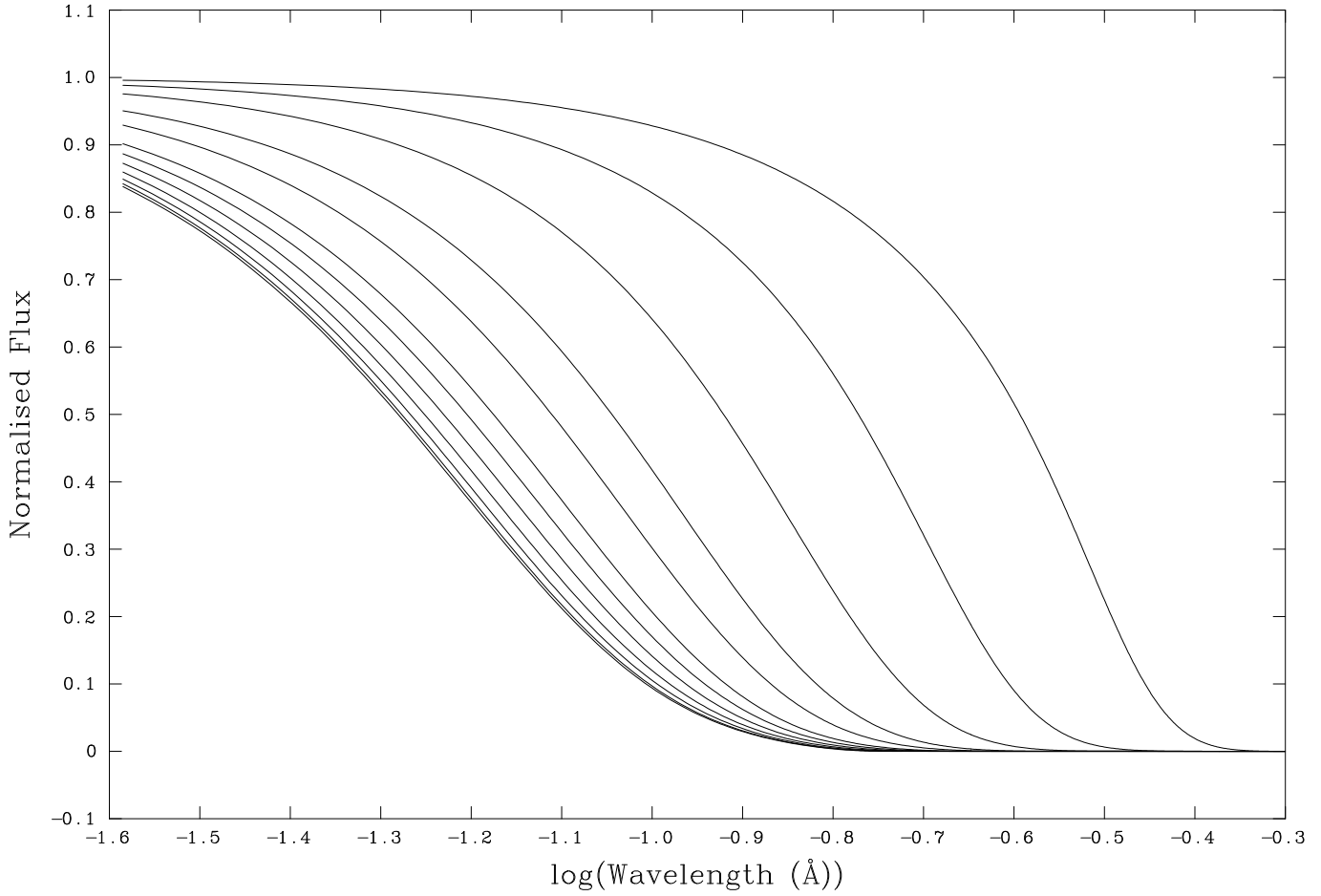


Fig. 4.— Cross-correlation function of GJ 1097 convolved with the rotational profiles for  $v \sin i$  values of 0.0 (left-most curve), 0.5, 1.0, 1.5, 2.0, 2.5, 3.0, 4.0, 5.0, 7.0, 10.0 and 15.0 (right-most curve)  $km s^{-1}$ . By superposing actual stellar data on these curves, we find that we can measure the broadening of our template cross-correlation profile (GJ 1097 for HARPS) down to  $v \sin i$  values of  $0.25 km s^{-1}$ . Here the curve corresponding to our detection threshold of  $1 km s^{-1}$  is clearly separated in the diagram from the zero-rotation limit.

are almost no differences for low values of  $v \sin i$  and large values of  $v \sin i$ . But for intermediate values  $3 < v \sin i < 7 \text{ km s}^{-1}$ , the differences can be large: this difference can be as large as  $0.9 \text{ km s}^{-1}$  for  $v \sin i$  at about  $4 \text{ km s}^{-1}$ . Therefore it is important to take into account limb-darkening effects when measuring  $v \sin i$  and  $P / \sin i$ .

### 5.3. Comparison with previous measurements

In order to further assess the precision of the rotational velocity measurements reported in this paper, we searched the literature for other  $v \sin i$  or rotational period  $P$  measurements for our M0, M2, M3 and M4 targets. We found several measurements of  $v \sin i$  (Vogt et al. 1983, Marcy & Chen 1992, Delfosse et al. 1998, Mohanty & Basri 2003) and  $P$  (Pizzolato et al. 2003, Kiraga & Stepień 2007, Irwin et al. 2011). We computed the  $v \sin i$  from the rotation periods  $P$  assuming  $\sin i = 1$ . We plot in Fig. 6 our best measurements versus the measurements from other spectrographs (e.g. SOPHIE as a function of HARPS, 7 measurements in the present sample of dM3 stars, see Table 2, and 19 in total) and the measurements from other authors (46 measurements). One can see in this figure that the overall agreement is good, even for sub- $\text{km s}^{-1}$  measures (13 measures). (The solid line in Fig. 6 indicates where the results would lie if the agreement were perfect.) The mean of the differences between our best measures and other measures are  $0.42 \text{ km s}^{-1}$  and  $1.13 \text{ km s}^{-1}$  for the slow rotators and the fast rotators respectively. This value for the slow rotators is presently lower than the  $3\sigma$  estimated above due to the uncertainty in the background of the cross-correlations. Furthermore, this figure allows us to expect that we should be able to measure  $v \sin i$  down to  $0.50 \text{ km s}^{-1}$  for our M dwarf samples, i.e. a factor of 2 better than our estimates given above. The value of  $1.13 \text{ km s}^{-1}$  for the fast rotators is much higher than our present estimates for these objects (see Table 2). Indeed, we should obtain the best precision for the fast rotators. The scatter of individual values in Fig. 6 relative to the perfect agreement line can be partly explained as follows: i) limb-darkening effects were not taken into account by all authors in the derivation of  $v \sin i$  values in the literature, and ii) we assumed  $\sin i = 1$  for some of the stars when in reality, the value of  $\sin i$  must in some cases be smaller than 1. In fact, in the case of fast rotators, different authors report differences of about  $1 \text{ km s}^{-1}$  between their observations of  $v \sin i$ : this might be due to the fact that

these highly active stars are spotted, and that the presence of large spots which can appear and disappear between different observing epochs yields varying values of  $v \sin i$ .

We note two large discrepancies between our measures and those of Kiraga & Stepień (2007) (not visible in Fig. 6). First, we found Gl 431 to be a rapid rotator  $v \sin i = 22.1 \text{ km s}^{-1}$ , in agreement with its strong CaII and  $H_\alpha$  emissions (Papers XVII and XVIII) whereas Kiraga & Stepień (2007) give a rotation period of 14.31 days ( $v \sin i \sim 1.5 \text{ km s}^{-1}$ ). Obviously their detection of the rotational modulation seems spurious. ii) for Gl 669A we have  $v \sin i = 1.86 \text{ km s}^{-1}$  whereas Kiraga & Stepień (2007) give a rotation period of 0.950 days ( $v \sin i \sim 28.5 \text{ km s}^{-1}$ ). Obviously, here again they have a spurious detection.

### 5.4. The distributions of the rotation periods

We have compiled all of our rotation periods from the combined sub-samples of dM0, dM2, dM3 and dM4 stars: the total number of stars is 277. We sum them all and plot a histogram of the number of stars as a function of the rotation period in Fig. 7. Our histogram shows 3 peaks: (i) fast rotators at periods close to 5 days; (ii) the largest peak at periods close to 15 days; (iii) a weaker peak at periods close to 23 days. In order to estimate the validity of this histogram, we overplot the histogram of the rotation periods reported by Nielsen et al. (2013) for a sample of more than 12,000 M dwarfs. Nielsen et al. obtained their results by analyzing photometric data from the Kepler spacecraft: in the presence of long-lived starspots, photometry allows a direct measurement of the rotation period, without the uncertainties associated with  $\sin i$ . In view of the  $\sin i$  factor, which cannot have a value in excess of unity, we expect that our histogram of  $P / \sin i$  will be skewed towards longer periods in comparison with the measurements of Nielsen et al.

Nevertheless, inspection of Fig. 7 indicates that the histogram of Nielsen et al. (2013) overlaps with ours in certain respects. Most importantly, the main peak occurs at about 15 days: in fact the median value of the Nielsen et al. histogram occurs at 15.4 days. This overlaps well with our largest peak. Moreover, a secondary (smaller) peak occurs in the Nielsen et al results at periods of 3-5 days, overlapping with our "fast rotator" peak. At longer periods, i.e. among the slow rotators, our distribution has a longer tail than the Nielsen et al. histogram, but this behaviour is to be expected based



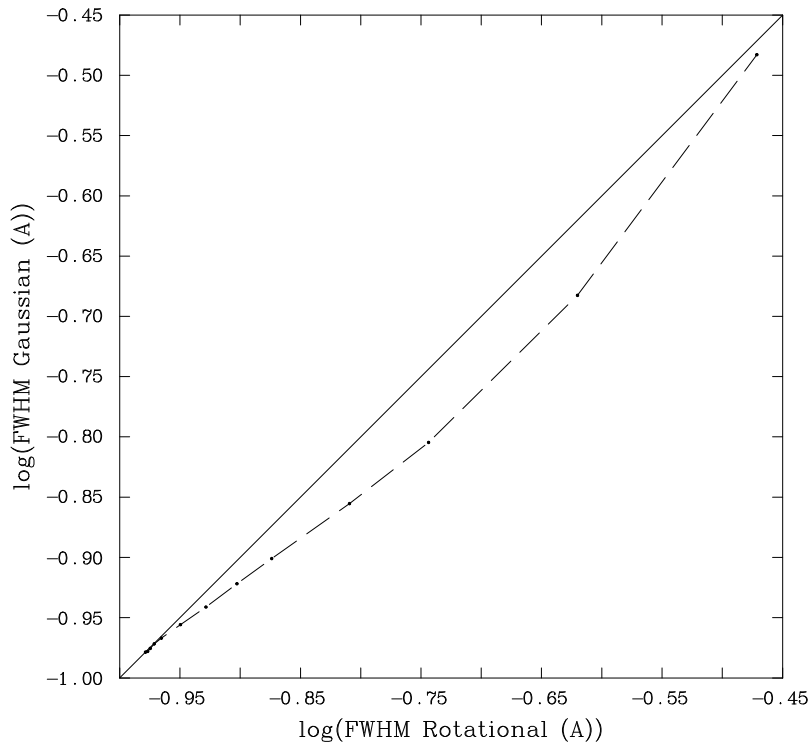


Fig. 5.— Dashed line: comparison of the FWHM of broadened profiles of GJ 1097 calculated by two different methods: (i) using our theoretical rotational profiles (see values on x-axis) and (ii) using Gaussian profiles (see values on y-axis). Solid line: results would lie along this line if both methods produced identical broadening. Along the dashed line, the Gaussian broadened profiles are systematically narrower than the theoretical rotational profiles.

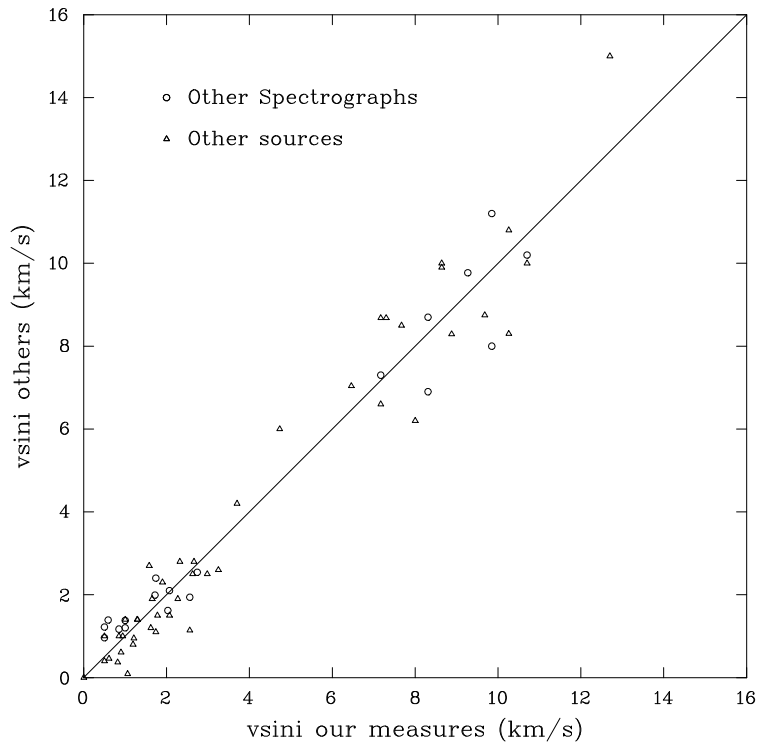


Fig. 6.— Comparison between our measurements of  $v \sin i$  (x-axis) and measurements of  $v \sin i$  from other spectrographs and from other authors (y-axis). Included in the plot are data for all of our sample M dwarfs (including subtypes M0, M2, M3 and M4). The solid line indicates perfect agreement between measurements.

on the  $\sin i$  factor in our data.

A separate investigation of rotational periods among a large sample of M dwarfs has also been reported by McQuillan et al. (2013), also using Kepler data. In a sample of 1570 M dwarfs, the distribution of rotation periods is found to be bimodal, with peaks at about 19 and 33 days. McQuillan et al use proper motion data to suggest that the two peaks correspond to stars of different ages, with the older group having the longer rotation periods. This interpretation suggests that the slower rotating stars may belong to the halo population, whereas the faster rotations may belong to the disk population. As we noted above (Section 2.2), in the present study, we calculate the period values (and the period distribution) *fordiskstaronly*: we do not include halo stars. This suggests that our sample of periods should include few (if any) halo stars: in view of this, we would not expect to recover the peak at 33 days reported by McQuillan et al. Only the 19 day peak in the McQuillan et al results should be compared to our results: this presumably corresponds to the 15 day peak in our data. The difference between the peak periods (19 vs 15 days) may be associated with the much larger sample of stars observed by McQuillan et al: the latter sample is larger than ours by a factor of 5-6, and may contain more halo stars than our sample.

Overall, allowing for significant differences in sample sizes, our results seem to agree rather well with the more precise results obtained from the rotational modulation for the larger number of M dwarfs which have been observed with Kepler.

The reason why we can attain precisions as good as those mentioned above in our dM3 stars is the same as for our earlier work on dM2 stars: our cross-correlation profiles have a very high S/N ratio (several hundred: see Fig. 3). This is due to the fact that the cross-correlations are based on combining the profiles of many spectral lines. It is therefore in theory possible to measure subtle differences between different cross-correlation profiles (see Fig. 4) of only a few percent. Our results can be compared to the noisier background in Reiners et al. (2012) where background noise is about 20 which limits their detection ability to  $v \sin i$  values in excess of  $3 \text{ km s}^{-1}$ .

## 6. Rotation of M3 dwarfs

In Fig. 8, the projected rotation periods  $P/\sin i$  are shown as a function of stellar radius. (Note the inverted scale on the vertical axis.) In order to

highlight differences between the less active (dM3) stars, the more active (dM3e) stars, and the subdwarfs (sdM3), we use different symbols for these different types of M3 dwarfs in Fig. 8. The solid line through dM3 and sdM3 data illustrates that  $P/\sin i$  tends to decrease (from 45 days to about 9 days) as the radius decreases (from  $0.6 R_{\odot}$  to  $0.2 R_{\odot}$ ). Such a trend was also found in our sample of dM4 stars, and also to some extent in our dM2 stellar sample. In our sample of dM3 stars, we have only a few subdwarfs, but the few which are in the sample do indeed have on average shorter rotation periods than the main sequence stars do. Our data indicate that, in spite of their probable older age, subwarfs rotate more rapidly than normal dwarfs. Although the results of Savcheva, West & Bochanski (2014) suggest that M type subdwarfs are not members of the halo unless they are "extreme" or "ultra" subdwarfs. Our results highlights the fact that magnetic braking mechanisms among early M dwarfs depend mainly on the stellar radius and mass (Houdebine et al. 2015); the magnetic braking mechanisms decrease more rapidly in efficiency with stellar radius than their efficiency integrated over age.

The study of the distributions of stellar rotation periods as a function of spectral type is particularly important for our understanding of stellar rotation dynamics. These distributions may provide essential new constraints for the mechanisms of magnetic braking. Fig. 9 illustrates the histogram of  $P/\sin i$  values which we have obtained in this paper for our sample of dM3 stars. In separate panels, we also present, for purposes of comparison, the corresponding histograms for our samples of dM2 and dM4 stars (data for which were reported in earlier papers). Inspection of the dM3 histogram indicates that our sample includes projected periods as long as 40-45 days, and as short as 1-2 days. It appears that the dM3 histogram contains one well defined peak, and perhaps also some smaller peaks. However, the statistics of small numbers may lead to only marginal significance for the smaller peaks. The dM3 histogram also contains several fast rotators: the two fastest rotators in our sample, Gl 896A and Gl 207.1 (with  $v \sin i = 14$  and  $9.5 \text{ km s}^{-1}$ ) are both dM3e stars. Thus, the stars which exhibit the fastest rotation are also stars with a high level of magnetic activity. This is consistent with the RAC. We consider the dM3 stars in our sample as slow rotators, while the dM3e stars are fast rotators, i.e. we consider the boundary where  $H_{\alpha}$  starts to go into emission as equivalent to a boundary between slow and fast rotation among M3

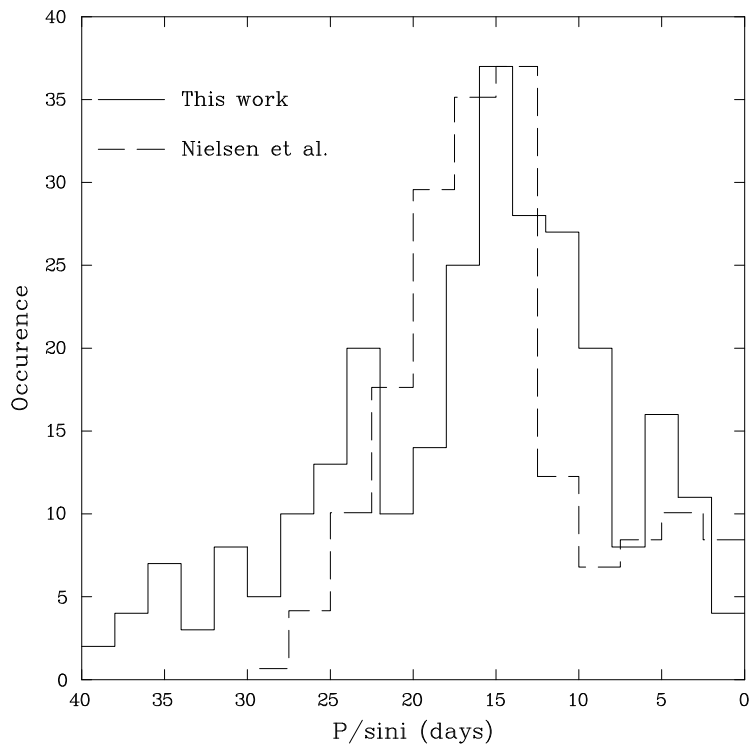


Fig. 7.— Solid curve: Number of stars in our sample of M dwarfs as a function of the rotation period. Included are all M dwarfs from the combined data for sub-types M0, M2, M3 and M4. Dashed curve: results of Nielsen et al. (2013) for a much larger sample of stars.

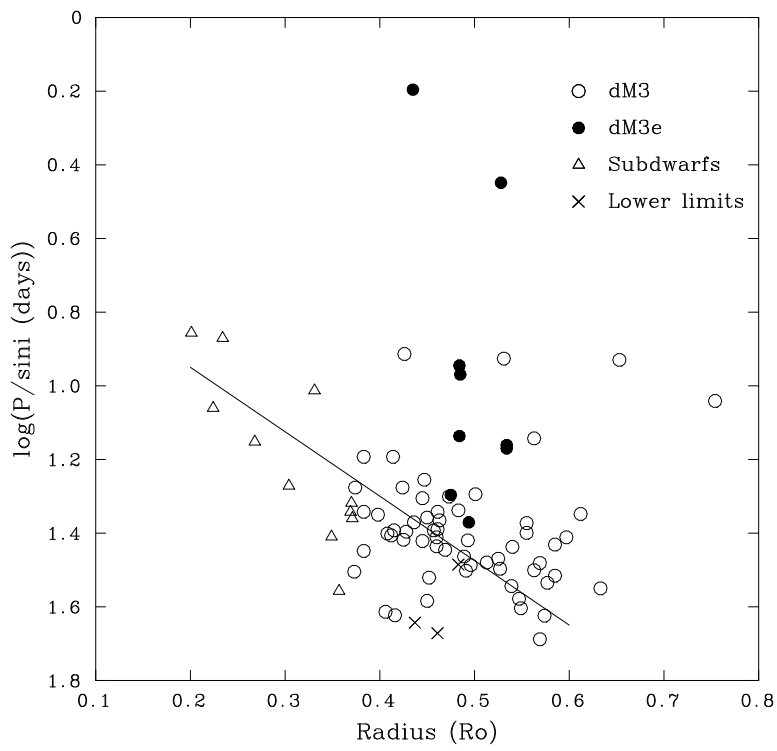


Fig. 8.—  $P/\sin i$  measurements as a function of stellar radius. Open circles: dM3 stars; filled circles: dM3e stars; triangles: sdM3; crosses: lower limits.

dwarfs.

Comparison of the dM3 and dM2 histograms indicates that our dM3 distribution extends over a broader range of periods than our dM2 distribution, despite the fact that their spectral classifications differ by only one decimal sub-type. For dM2 stars we observe that the distribution for slow rotators is rather compact, with the main peak around 11 days, and almost no stars at periods longer than 18 days. In contrast to this, in the dM3 histogram, the largest peak is attained at a period of 23 days and there are numerous stars with even longer periods.

Comparison between the dM3 histogram and the dM4 histogram reveals even more striking differences between stars which also differ by only one decimal sub-type. For dM4 stars, the distribution is extremely compact with a maximum around 14 days, with possibly a second maximum around 6 days, and no stars at all with periods longer than 18 days.

In view of these differences among the histograms, the results in Fig. 9 suggest that rotational properties of M dwarfs do not vary in a manner which could be described simply as monotonic as we move from dM2 through dM3 to dM4 spectral sub-types. Our results indicate that our sample of dM3 stars contains many stars which have rotation periods which are clearly longer than those of any of the dM2 and dM4 stars in our samples.

To quantify the differences between rotational properties of the various decimal sub-types of dM stars, we consider the average (projected) rotation period  $P/\sin i$  (*ave*) of the stars in our various sub-samples of slow rotators (i.e. excluding spectroscopic binaries, subdwarfs, and active chromosphere stars). For dM3 stars, including all of the inactive stars in our sample (numbering 49 stars), we find that averaging of the individual  $P/\sin i$  measurements leads to  $P/\sin i$  (*ave*) = 25.8 days. If we include only dM3 stars out to a maximum distance of 13 pc (where our sample is closer to complete), we find  $P/\sin i$  (*ave*) = 23.5 for a sample of 25 stars (i.e. still excluding spectroscopic binaries, sdM3 and dM3e stars). These two values are very close, within  $\pm 1.1$  days of an average of 24.65 days. Therefore the bias in our sample towards the brightest dM3 stars does not appear to have a significant selection effect on the value of  $P/\sin i$  (*ave*). In order to place an error bar on our estimates of  $P/\sin i$  (*ave*), we first calculate an individual error for the  $P/\sin i$  value for each of our 49 dM3 stars. To do this, we include the errors on the absolute magnitudes and in the radius

measurements (Table 1), and we also include the errors on the  $v \sin i$  measurements (Table 2). Combining these errors, we derive the errors listed in Table 2 for each of the individual  $P/\sin i$  measurements for our 49 stars. We then calculated the mean of these individual errors: we found the mean errors below and above the mean to be  $\sigma = -5.98 \text{ days}$  and  $\sigma = +13.8 \text{ days}$ . Using these mean errors for the individual values of  $P/\sin i$  for 49 stars, we obtained a mean error on the average  $P/\sin i$  (*ave*) for 49 stars by dividing the mean individual errors by  $\sqrt{49}$ . In this way, we find errors on  $P/\sin i$  (*ave*) ranging from -0.85 days to +1.97 days. Treating these as standard deviations on  $P/\sin i$  (*ave*), we conclude that the  $3\sigma$  error bars on our computed values of  $P/\sin i$  (*ave*) are -2.56 days and +5.9 days. These error bars are included in Fig. 10 in association with the plotted value of  $P/\sin i$  (*ave*) = 25.8 days for dM3 stars.

Turning now to our samples of dM2 and dM4 stars, we find that the mean projected period  $P/\sin i$  (*ave*) has values of 14.4 days and 11.4 days respectively. In order to assign error bars to these values, we considered the average  $v \sin i$  and average radius for our sub-samples of dM2 and dM4 stars. An upper value of the error on the mean periods is then given by the standard error on  $v \sin i$ . We found that the mean  $v \sin i$  is  $2.41 \text{ km s}^{-1}$  and  $1.57 \text{ km s}^{-1}$  for dM2 and dM4 stars respectively in our samples. The mean radii are  $0.623 R_{\odot}$ ,  $0.490 R_{\odot}$  and  $0.366 R_{\odot}$  for dM2, dM3 and dM4 stars respectively. These yield uncertainties of  $\pm 1.44$  days and  $\pm 1.89$  days on the  $P/\sin i$  (*ave*) values for dM2 and dM4 stars respectively. Along the same lines, we found that the mean radii are  $0.815 R_{\odot}$  and  $0.711 R_{\odot}$ , and the mean  $v \sin i$  are  $1.62 \text{ km s}^{-1}$  and  $2.28 \text{ km s}^{-1}$  for dK5 and dM0 stars respectively. This gives uncertainties of  $\pm 6.00$  days and  $\pm 2.84$  days for  $P/\sin i$  (*ave*) in dK5 stars and dM0 stars respectively. The values of  $P/\sin i$  (*ave*) and their error bars are plotted for our samples of dK5, dM0, dM2, dM3, and dM4 stars in Figure 10.

On an observational selection note, we point out that some of our detections of  $v \sin i$  lie below the  $3\sigma$  threshold of  $0.95 \text{ km s}^{-1}$  for HARPS and  $1.22 \text{ km s}^{-1}$  for SOPHIE. As a result, the values of  $P/\sin i$  (*ave*) we give above are lower limits to the real figure of the average rotation period for dM stars. However, we see no reason why this should affect dM3 stars more than dM2 or dM4 stars. Therefore, there should be no significant effect on the principal conclusion which we reach in this *differential* study between neighbouring

spectral sub-types: the value of  $P/\sin i$  (*ave*) for dM3 stars is abnormally large compared to the values for dM2 and dM4 stars.

If there existed a monotonic decrease in  $P/\sin i$  (*ave*) as the spectral type moved to later values, then given the values of 14.4 days and 11.4 days for dM2 and dM4 stars, one would expect dM3 stars to have an average rotation period of 12.9 days. Instead of that, our results indicate that dM3 stars rotate more slowly than this expectation, by an amount  $25.8-12.9 = +12.9$  days. Compared to our estimate above of the standard deviation of  $+1.97$  days (towards longer periods), the deviation of dM3 stars from monotonic behaviour between dM2, dM3 and dM4 has a statistical significance of  $(6-7)\sigma$ . This suggests that there is something happening at spectral type dM3 which deviates significantly from the monotonic behaviour demonstrated by K5, M0, M2, and M4 dwarfs.

We conclude that on average, dM3 stars rotate slower than expected when compared with stars of immediately adjacent spectral sub-type. Moreover, the period distribution of dM3 stars exhibits a stronger skewing towards longer periods, with some members of the sub-sample rotating as slowly as 40-45 days. These slow rotations are consistent with the low activity levels of dM3 stars as measured in the Ca II lines (Houdebine et al. 2015).

So far, we have discussed the rotational properties of the slow rotators among our dM2, dM3, and dM4 samples. Now let us turn to the more active stars, i.e. dM2e, dM3e, and dM4e, and ask: is there any evidence to indicate that the unusually slow rotation of M3 stars is also present among the active stars? To address this topic, we have analysed independently the mean rotation periods for active stars (i.e. M dwarfs with  $H_\alpha$  in emission). We find  $P/\sin i$  (*ave*) =  $4.22\pm 0.26$ ,  $2.82\pm 0.19$ ,  $4.11\pm 0.20$ ,  $10.3\pm 1.34$  and  $6.32\pm 0.30$  days for dK5, dM0, dM2, dM3 and dM4 stars respectively. The value for dM0 stars is not trustworthy, because of the smallness of the sample. The numerical values of  $P/\sin i$  (*ave*) for other sub-samples (dK5e, dM2e, dM3e, dM4e) suggest that for the fast rotators,  $P/\sin i$  (*ave*) tends to increase towards later spectral types. This is the opposite trend to that of the slow rotators. One can explain this if one considers that dM4e stars stay longer at a high level of activity than dK5e stars (see RM). In other words, on average, the sample of active stars gets older as the spectral type increases (RM). Despite this behaviour, our averages indicate that dM3e stars once again stand apart from

immediately adjacent decimal subtypes in the following sense: the dM3e stars have a significantly longer rotation period.

Thus, the relatively long rotation period of M3 stars (relative to M2 and M4) emerges in our data for both slow rotators (dM3) and fast rotators (dM3e). Thus, whether we consider dM3e stars (relatively young) or dM3 stars (relatively older), some process of magnetic braking has slowed M3 stars down more efficiently than the adjoining M2 and M4 stars.

A summary of our results is illustrated in Fig. 10, where the mean rotation period  $P/\sin i$  (*ave*) is plotted as a function of  $(R-I)_c$ , with labels attached to the appropriate spectral sub-type. Fig. 10 indicates that, in an overall sense, there is a trend in  $P/\sin i$  (*ave*) to decrease from longer than 30 days to about 10 days as the spectral sub-type increases from dK5 to dM4. But a departure from this trend occurs among the dM3 stars: there, the value of  $P/\sin i$  (*ave*) rises to a peak which stands well above the value one might expect from a simple interpolation between dM2 and dM4. The slowest rotators in Fig. 10 are the dK5 stars with a mean rotation period longer than 30 days. (This value is actually a lower limit because the  $v\sin i$  values of many dK5 stars were below the detection limit of  $1\text{ km s}^{-1}$ .) Overall, the long periods of dK5 stars indicate that rotational braking has been quite efficient for dK5 stars, whereas the short periods of dM4 stars indicate that rotational braking has *not* been as efficient for those stars. The dM3 stars do not fit into this trend: the dM3 data suggest that at dM3, the braking mechanism is *more effective than the data for dM2 and dM4 stars would lead us to expect*.

The results in Fig 10 may provide an important constraint on the rotational braking mechanism, in particular at the fully convective threshold. In the next section, we turn to a discussion of this topic.

## 7. Discussion

The results in Fig. 9 and Fig. 10 suggest that something unusual happens to the rotational properties of dwarfs at dM3, presumably associated with a change in  $dJ/dt$ . In this section, we review the quantities which determine  $dJ/dt$  in order to ask: what might be unusual about M3? We shall discuss several of the factors mentioned by RM as worthy of attention (see Section 1.4).

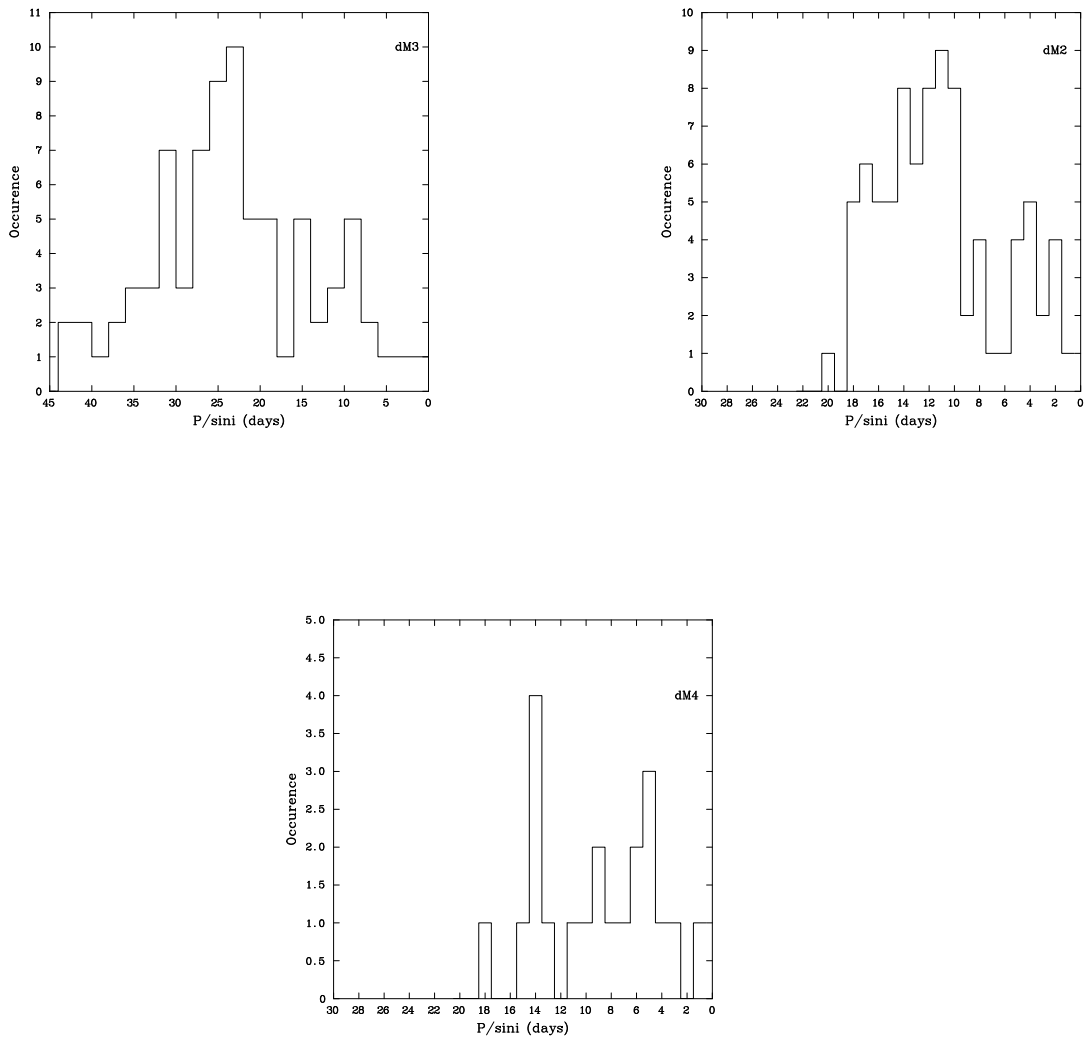


Fig. 9.— Histograms of  $P/\sin i$  for stars of spectral sub-types dM3, dM2, and dM4. Note that dM3 stars have rotational periods which extend to larger values than dM2 stars and dM4 stars.



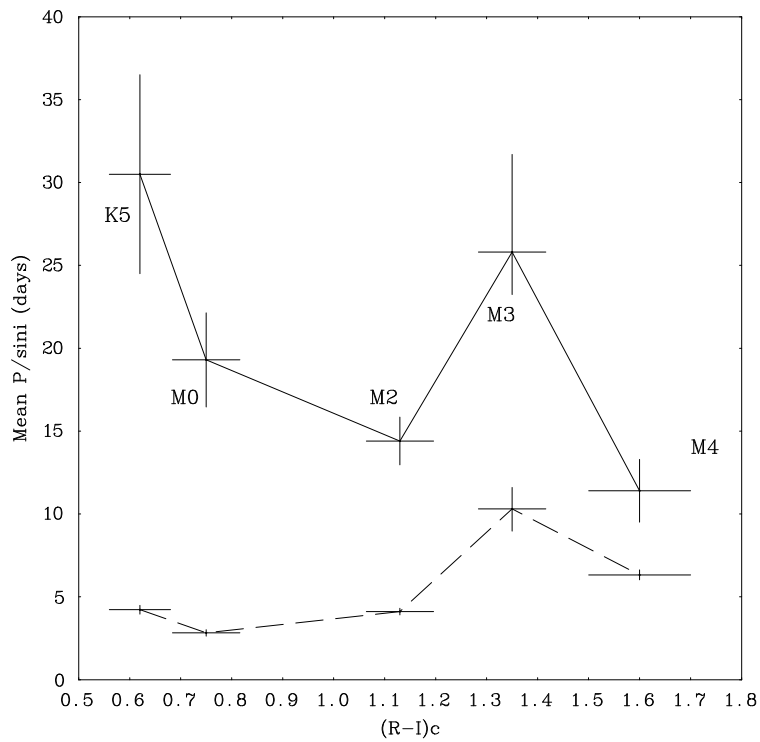


Fig. 10.— Mean  $P/sini$  values of inactive (continuous line) and active (dashed line) dwarfs as a function of  $(R-I)_c$ . Note that, although there is an overall trend to shorter periods as spectral type increases, there is a significant departure from this trend at dM3. Theoretically, M3 is where transition to complete convection is thought to occur.

### 7.1. Contributions to $dJ/dt$ : $\dot{M}$

Two factors determine  $dJ/dt$  (see Section 1.2.2):  $\dot{M}$  and the lever arm length  $D = R_A$  (the Alfvénic radius) of enforced co-rotation. As regards  $\dot{M}$ , there are no reliable direct measures for M dwarfs. However, indirect information about  $\dot{M}$  comes from studies of a "hydrogen wall" which accumulates in the interaction between the wind and the interstellar medium. Wood (2006) has analyzed the available data and concludes that in the M dwarfs,  $\dot{M}$  may be smaller than the solar value.

### 7.2. Contributions to $dJ/dt$ : the "lever arm" $D$

In all stars,  $D$  can certainly not be  $< R_*$ . But  $D$  may be  $\gg R_*$  if the  $B$  field is extended and strong. The larger  $D$ , the larger  $dJ/dt$  for a given  $\dot{M}$ . In the solar wind, scintillation data suggest  $D \approx (15-20)R_\odot$  (e.g. Mullan 1990). In M dwarfs,  $D$  is very uncertain because  $B$  is difficult to measure *in the wind*. On the *surface* of an M dwarf, the large-scale fields  $B$  are as strong as 1-4 kG (Saar, 1996; Reiners et al 2009), i.e. 100 times stronger than the large-scale (polar) fields in the Sun. As a result, we expect that  $D$  in M dwarfs may greatly exceed the solar value, thereby contributing to larger  $dJ/dt$ .

However, it is not merely the strength of  $B$  at the surface which contributes to  $D$ : the radial behaviour  $B(r)$  (i.e. the topology) is also important. Some M dwarfs are found to have dipole (global) topology (Donati et al. 2006), whereas others have small-scale (multipole, active regions) topology (Morin et al. 2010). Multipole fields of degree  $l$  fall off in strength with increasing radial distance as  $1/r^{2+l}$ . Dipoles ( $l = 1$ ) fall off as  $1/r^3$ , while quadrupole ( $l = 2$ ) and octupole ( $l = 3$ ) fall off  $1/r^4$  and  $1/r^5$ . Thus, multipoles are so strongly radial dependent that they tend to "close in on themselves" quite close to the surface of the star. Thus, multipoles have smaller "lever arms" than dipoles. Other things being equal,  $dJ/dt$  is smaller in a multipole field. To understand why some M dwarfs possess dipolar fields, while others possess multipolar fields, Gastine et al (2012) have used a dynamo model in a deep convective envelope to show that fast (slow) rotators tend to favor dipole (multipole) fields. In the present paper, with our deliberate choice of slow rotators, we should be dealing mainly with multipolar fields, i.e. stars where the sizes of active region loops will play a role in determining the lever arm  $D$ .

When we discuss magnetic topology in M dwarfs, we need to ask: does the topology change from one side of the TTCC to the other? Shulyak et al (2014) have discussed this issue by observing 4 stars near the TTCC: but they reported "no difference between the field distribution of partially and fully convective stars". We will discuss this result below (Section 7.6).

### 7.3. The value of $D$ and its relationship to magnetic loop lengths

In the presence of multipole fields, it seems plausible that the value of  $D$  may be determined by the length of the largest closed loops. In the solar corona, X-ray images indicate that the maximum height of closed loops is  $\leq (0.1 - 0.5)R_\odot$ . Can we estimate loop lengths in M dwarfs? Mullan et al. (2006) have reported a study of flaring loops in which the parameters of flare light curves allow extraction of loop lengths. In M dwarfs with colours which are redder than a certain limit, the loop lengths (expressed in terms of  $R_*$ ) were found to be several times larger than in solar-like stars. The onset of larger loops in cooler M dwarfs, with the associated increase in  $D$ , would contribute to an *increase* in  $dJ/dt$ , i.e. an increase in the ability to slow down stellar rotation to longer periods. Might this be related to the abnormal rotational properties of dM3 stars which we have identified in the present paper? The answer depends on precisely where the increase of loop lengths occurs in M dwarfs.

### 7.4. At what spectral type do large loop lengths set in among M dwarfs?

Mullan et al (2006) report that long loops set in at  $B-V = 1.4-1.5$ . Unfortunately,  $B-V$  values change so slowly between M0 and M4 that the above  $B-V$  range may lie anywhere between M0 and M4. However, Mullan et al. (2006) also report that long loops set in at  $V-I = 2.1-2.3$ . According to the online website <http://www.stsci.edu/~inr/intrins.html> the values of  $V-I$  at M2, M3, and M4 are 2.06, 2.24, and 2.43. Thus the onset of long loops occurs later than M2 and earlier than M4. The best fit is M3.

### 7.5. TTCC and dynamo activity

Dynamo activity in low mass stars is expected to change its properties at the TTCC. In stars with radiative cores, an interface dynamo can operate. But when the star is completely convective, such a dynamo

is impossible. This has long suggested that the dynamo should undergo a change of regime across the TTCC, perhaps to a distributed dynamo (e.g. Mullan and MacDonald 2001). Surprisingly, no evidence for such a change can be seen in the best X-ray data (Mullan and MacDonald 2001). But perhaps the X-ray data is not the best place to look for a change of dynamo regime. Where else might we look?

### 7.6. TTCC and loop lengths

Since the increase in loop length reported by Mullan et al (2006) occurs at M3, and this is the spectral type associated with the theoretical prediction of the TTCC, we suggest that an increase in loop length is associated with a change in dynamo regime at the TTCC. Even if  $\dot{M}$  did not change from M2 to M3, an increase in loop length in going from M2 to M3 would result in a sudden increase in  $D$ , with a concomitant increase in  $dJ/dt$ . This would cause more effective braking of stellar rotation at M3 at the TTCC compared to earlier M dwarfs, with their smaller loops. This could explain why the mean  $P/\sin i$  in Fig. 10 is longer for M3 stars than for M2 stars.

What about M dwarfs later than M3? They also have large loop lengths (Mullan et al. 2006), so should they not also have long rotation periods? The answer would be yes, if  $\dot{M}$  were the same at M4 as at M3. However, the (scant) data available from the study of Wood (1996) hints that  $\dot{M}$  may tend towards smaller values at later spectral types. To the extent that this is true, the magnitude of  $dJ/dt$  would become smaller at spectral type M4 even if the loop lengths remained as large as those at M3. In the presence of reduced  $dJ/dt$ , the M4 stars would be expected to rotate faster than M3 stars. This is consistent with the results which were shown above in Fig. 10.

Finally, if M3 is indeed the location of the TTCC, we can understand better the conclusions of Shulyak et al (2014), who reported that they found "no difference between the field distributions" in their sample of 4 stars. The fact is, their target stars were all of spectral type M3.5 or later, i.e. we would classify all 4 stars as fully convective. This could explain why all 4 stars have similar field distributions.

## 8. Conclusion

In this paper, we have presented values of projected rotational velocity  $v \sin i$  for a sample of 82 stars belonging to the narrow spectral sub-type dM3. The ve-

locities were extracted from archival spectra which had been obtained by observers using two spectrographs designed to be among the stablest and highest resolution instruments currently available. These instruments allowed us to determine values of  $v \sin i$  down to, or even somewhat below,  $1 \text{ km s}^{-1}$ . In order to achieve such high resolution and precision, we used a cross-correlation technique which fits the line profiles of hundreds of spectral lines. In earlier papers by one of us (E.R.H.), the cross-correlation technique has also been used to obtain  $v \sin i$  for stars of spectral sub-types dK5, dM2, and dM4. Comparison of our  $v \sin i$  values with results obtained by other observers for overlapping targets shows excellent agreement.

Combining our values of  $v \sin i$  with stellar radii for each star, we obtain a "projected rotational period"  $P/\sin i$  for each star in our dM3 sample. A histogram of  $P/\sin i$  for our dM3 sample spans a range from as short as 1-2 days to as long as 40-45 days, with a peak at 23 days. For the 49 slowly rotating dM3 stars in our sample (i.e. excluding dM3e stars, subdwarf sdM3 stars, and spectroscopic binaries), we find that the mean  $P/\sin i$  is  $P/\sin i (\text{ave}) = 25.8$  days. We estimate that the  $3\sigma$  uncertainties in this estimate are (-2.56, +5.9) days.

In view of the availability of earlier papers on rotational properties of several spectral sub-types, we have undertaken in this paper a detailed comparison between the rotational properties of dM3 stars and those of dK5, dM0, dM2, and dM4. We find that the histograms of  $P/\sin i$  for our samples of dM2 and dM4 stars are considerably narrower than for our dM3 sample. In particular, the dM3 rotational distribution contains a larger number of slow rotators than the neighbouring sub-types. Quantitatively, we find that the values of  $P/\sin i (\text{ave})$  for dM2 and dM4 stars are 14.4 and 11.4 days respectively. Linear interpolation between these two values suggests that dM3 stars might be expected to have  $P/\sin i (\text{ave}) = 12.9$  days: but this expectation is shorter by several  $\sigma$  than the value we have actually derived for  $P/\sin i (\text{ave})$  in dM3 stars. We conclude that the dM3 stars in our sample have been subjected to braking which is significantly more effective than the braking which has occurred in the adjacent spectral sub-types dM2 or dM4. We can think of no observational selection effect which would cause our dM3 sample to be spuriously affected in this way relative to our dM2 and dM4 samples: all samples were chosen from the same sets of archival data.

In an attempt to understand why braking of stellar

rotation might be different at dM3 than at dM2 or dM4, we note that magnetic loop lengths obtained from analysis of flare light curves (Mullan et al. 2006) increase to longer values at particular values of B-V and V-I colours. Interestingly, the V-I colour at which the loop sizes increase turns out to be spectral sub-type M3. To the extent that these two factors (rotation, loop length) are not merely coincidental, we regard the occurrence of both at sub-type M3 as an important conclusion of the present paper.

Especially significant is the fact that stellar structure theory predicts that stars on the main sequence should make a transition to complete convection (TTCC) at spectral type M3. It has often been speculated that a change in dynamo regime probably occurs at the TTCC: this could explain why loop lengths change at M3. In this context, we have proposed a possible explanation (Section 7.6) why the rotational properties of dwarfs might exhibit an abnormality at M3 relative to adjacent spectral sub-types.

The speculated switch in dynamo regime at the TTCC might be testable if further observational evidence were to reveal some other unusual property of dM3 stars relative to their neighbours (dM2 and dM4 stars). One possibility for such a test involves the frequencies of p-modes. It is known that magnetic fields inside a star cause structural changes which result in systematic shifts of p-mode frequencies (e.g. Mullan et al. 2007). A star with an interface dynamo (ID) located deep in the interior of the star might give rise to different magnetically-induced structural changes from those in a star with a distributed dynamo (DD) where fields are generated by small-scale turbulent processes throughout the convection zone (Durney et al. 1993). If the differences in structural changes between ID and DD turn out to be large enough, a study of frequency shifts among p-modes in dM2, dM3 and dM4 stars might help to strengthen the case for a switch in the dynamo regime at M3.

#### acknowledgements

The authors thank an anonymous referee for detailed and constructive comments which have helped to improve the paper. This research has made use of the SIMBAD database, operated at CDS, Strasbourg, France. DJM is supported in part by the NASA Space Grant program. The authors acknowledge the availability of the data made by the European Southern Observatory and Observatoire de Haute Provence.

#### REFERENCES

- Bessel, M.S. 1979, *PASP* 91, 589.
- Bessel, M.S. 1990, *A&A Sup. Ser.* 83, 357
- Booth, J., Caruso, J., Weis, E.W. 1988, *PASP* 100, 749
- Bouvier, J. 1990, *AJ* 99, 946
- Browning, M., Basri, G., Marcy, G.W., West, A.A. & Zhang, J. 2010, *AJ* 139, 504
- Cram, L. E. and Mullan D. J. 1979 *ApJ* 234, 579
- Dawson, P.C., Forbes, D. 1992, *AJ* 103, 2063
- Delfosse, X., Forveille, T., Perrier, C., Mayor, M., 1998, *A&A* 331, 581
- Donati, J, Forveille, T., Cameron, A. C. et al. 2006, *Science* 311, 633
- Durney, B.R., De Young, D.S. and Roxburgh, I.W. 1993, *Solar Phys.* 145, 207
- Eggen, O.J., 1974, *PASP* 86, 697
- Eggen, O.J., 1976a, *ApJS* 30, 351
- Eggen, O.J., 1976b, *ApJ* 204, 101
- Eggen, O.J., 1978, *ApJS* 37, 251
- Eggen, O.J., 1979, *ApJS* 39, 89
- Eggen, O.J., 1980, *ApJS* 43, 457
- Eggen, O.J., 1987, *AJ* 92, 379
- Feigelson, E.D., Gafney III, J.A., Garmire, G., Hillebrand, L.A., Townsley, L. 2003, *ApJ* 584, 911
- Fleming, T.A., Gioia, I.M. & Maccacaro, T. 1989, *ApJ* 340, 1011
- Gastine, T., Duarte, L. & Wicht, J. 2012, *A&A* 546, A19
- Hartmann, L.W., Baliunas, S.L., Duncan, D.K. & Noyes, R.W. 1984, *ApJ* 279, 778
- Houdebine, E.R. 2008, *MNRAS* 390, 1081 (Paper VII)
- Houdebine, E.R. 2009a, *MNRAS* 397, 2133 (Paper XII)
- Houdebine, E.R. 2009b, *MNRAS* 400, 238 (Paper XIII)

- Houdebine, E.R. 2010a, MNRAS 509, 65 (Paper IX)
- Houdebine, E.R. 2010b, MNRAS 407, 1657 (Paper XIV)
- Houdebine, E.R. 2010c, MNRAS 403, 2157 (Paper X)
- Houdebine, E.R. 2011a, MNRAS 411, 2259 (Paper XV)
- Houdebine, E.R. 2011b, MNRAS 416, 2233 (Paper XVI)
- Houdebine, E.R. 2012a, MNRAS 421, 3180 (Paper XVII)
- Houdebine, E.R. 2012b, MNRAS 421, 3189 (Paper XVIII)
- Houdebine, E.R. 2012c, MNRAS 421, 3180 (Paper XVII)
- Houdebine, E.R. & Doyle, G.J. 1994, in *Cool Stars; Stellar Systems; and the Sun; Eighth Cambridge Workshop, Proceedings, held in Athens, Georgia*, Caillault J.P. ed., ASPCS, Vol. 64, p. 423
- Houdebine, E.R. & Stempels, H.C. 1997, A&A (Paper VI)
- Houdebine, E.R., Butler, C.J., Garcia-Alvarez, D., Telting, J. 2012, MNRAS 426, 159 (Paper XIX)
- Houdebine, E.R., Paletou, F., Mullan, D.J. 2015, in preparation
- Irwin, J., Berta, Z.K., Burke, C.J., Charbonneau, D., Nutzman, P., West, A.A. & Falco, E.E. 2011, ApJ 727, 56
- Jeffries, R.D., Totten, E.J., James, D.J. 2000, MNRAS 316, 950
- Jones, H.R.A., Longmore, A.J., Jameson, R.F., Mountain, C.M., 1994, MNRAS, 267, 413
- Kenyon, S.J. & Hartmann, L. 1995, ApJ Suppl. Ser. 101, 117
- Kiraga, M. & Stepien, K. 2007, Acta Astron. 57, 149
- Leggett, S.K., 1992, ApJS 82, 351
- Leggett, S.K., Hawkins, M.R.S. 1988, MNRAS 234, 1065
- MacDonald, J. and Mullan, D.J. 2003, ApJ 598, 560
- Marcy, G.W. & Chen, G.H. 1992, ApJ 390, 550
- Marilli, E., Catalano, S. & Trigilio, C. 1986, A&A 167, 297
- Mayor et al. 2003, The Messenger, 114, 20
- McQuillan, A., Aigrain, S. & Mazeh, T. 2013, MNRAS 432, 1203
- Mohanty, S. & Basri, G. 2003, ApJ 583, 451
- Montesinos, B., Thomas, J.H., Ventura, P. & Mazzitelli, I. 2001, MNRAS 326, 877
- Morin, J., Donati, J., Petit, P. et al. 2010, MNRAS, 407, 2269
- Mullan, D.J. 1984, ApJ 282, 603.
- Mullan, D.J., 1990, A&A 232, 520
- Mullan, D.J. & MacDonald, J. 2001, ApJ 559, 353.
- Mullan, D.J., MacDonald, J. & Townsend, R.H.D. 2007, ApJ 670, 1420
- Mullan, D.J. , Mathioudakis, M., Bloomfield, D.S., & Christian, D.J. 2006, ApJ Suppl. 164, 173
- Nielsen, M.B., Gizon, L., Schunker, H., Karoff, C. 2013, A&A 557, L10
- Noyes, R.W., Hartmann, S.W., Baliunas, S.L., Duncan, D.K. & Vaughan, A.H. 1984, ApJ 279, 763
- Pallavicini, R., Golub, L., Rosner, R., Vaiana, G.S., Ayres, T. & Linsky, J.L. 1981, ApJ 248, 279
- Patten, B.M. & Simon, T. 1996, ApJS 106, 489
- Pizzolato, N., Maggio, A., Micela, G., Sciortino, S., Ventura, P. 2003, A&A 397, 147
- Perruchot et al. 2008, in McLean I.S., Casali M.M., eds; Proc. SPIE Vol. 7014, *Ground-Based and Airborne Instrumentation for Astronomy II*. SPIE, Bellingham, p. 70140J
- Reiners, A., 2007, A&A 467, 259
- Reiners, A., Basri, G., & Browning, M. 2009, ApJ, 692, 538
- Reiners, A., Nandan, J., Goldman, B. 2012, AJ 143, 93

- Reiners, A., Schussler, M. & Passegger, V.M., 2014  
arXiv 1408, 6111
- Rodgers, A.W., Eggen, O.J., 1974, PASP 86, 742
- Saar, S. H. 1996, in Stellar Surface Structure, eds. K.  
G. Strassmeier and J. L. Linsky, Kluwer, Dordrecht,  
p. 237
- Savcheva, A.S., West, A.A., Bochanski, J.J. 2014, ApJ  
794, 145
- Shulyak, D., Reiners, A. et al., 2014, A&A 563, A35
- Simon, T.; Fekel, F.C., Jr. 1987, ApJ 316, 434
- Soderblom, D.R. 1982, ApJ 263, 239
- Stauffer, J. R. and Hartmann, L. W. 1986, ApJ Suppl  
61, 631
- Ungren, A.R., Lu, P.K. 1986, AJ 92, 903
- Veeder, G.J. 1974, AJ 79, 1056
- Vilhu, O. & Rucinski, S. M., 1983, A&A 127, 5
- Vogt, S.S., Soderblom, D.R., Penrod, G.D. 1983, ApJ  
269, 250
- Walter, F. M. 1982, ApJ 253, 745
- Weis, E.W. 1991a, AJ 101, 1882
- Weis, E.W. 1991b, AJ 102, 1795
- Weis, E.W. 1993, AJ 105, 1962
- Weis, E.W., Ungren, A.R. 1982, PASP 94, 821
- West, A. A., Hawley, S. L., Bochanski, J. J., et al.  
2008, AJ 135, 785
- Wood, B. 2006, in The Physics of the Heliospheric  
Boundaries, eds. V. V. Izmodenov and R. Kallen-  
bach, ESA/ISSI, p. 335
- Yadav, R. K., Gastine, T., Christensen, U. R., &  
Duarte, L. 2013, ApJ 774, 6